ISSN No:-2456-2165 https://doi.org/10.38124/ijisrt/IJISRT24MAY479

Optimized Design of a 50kva Transformer for Ferroresonance Mitigation and Power Quality Enhancement

Jibrin Abdullahi[1]; Aminu Alhaji Abdulhamid[2]
Department of Electrical and Electronic Engineering Technology,
Isa Mustapha Agwai I Polytechnic, Lafia

Abstract:- This study investigates transformer performance by combining Finite Element Method (FEM) and MATLAB/Simulink modeling and simulations, focusing on efficiency, core losses, and ferroresonance phenomena. Analyzing transformer behaviors, including anisotropy and non-linearity, via FEM simulations and analytical formulations reveals significant insights. Grounded in the Nonlinear Inductance Electromagnetic Transformer (NIEMT) Model and Maxwell's equations, the study models core losses, reluctivity, and relative permeability to capture magnetic flux dynamics. MATLAB/Simulink models simulate ferroresonance effects on distribution transformer behavior in low voltage power systems. Findings highlight differences in ferroresonance resilience: Total Harmonic Distortion (THD) in the baseline transformer is up to 30% higher than in the optimized transformer. Additionally, respective flux density and losses are 40% and 2.55% higher in the baseline compared to the optimized transformer, demonstrating how design changes enhance performance. Experimental validation underscores practical implications, while ferroresonance analysis identifies stability challenges and mitigation strategies. This research offers valuable insights for transformer design and power system stability enhancement.

Keywords:- *Finite Element Method (FEM), Ferroresonance Phenomena, Anisotropy, NIEMT Model, Maxwell's Equations, Total Harmonic Distortion (THD).*

I. INTRODUCTION

Transformers are pivotal in power systems, facilitating efficient energy transmission and distribution [20]. They are integral to various applications, including power plants, substations, and residential areas, supporting the advancement of clean energy technologies [21]. Technological advancements in transformers aim to improve efficiency, performance, and environmental responsibility, essential for modernizing power grids and integrating renewable energy sources [22].

Despite their significance, transformers face challenges such as ferroresonance, a non-linear resonance phenomenon that poses threats to their operation and reliability [25]. Ferroresonance triggers harmful electrical behavior, leading to increased losses and potential transformer failures [4]. Mitigating ferroresonance is crucial for ensuring power system reliability and efficiency [26].

However, existing transformer designs may not fully address ferroresonance concerns [24]. Optimizing transformer designs is essential to enhance performance and minimize risks associated with ferroresonance [27]. The Finite Element method (FEM) offers a systematic approach to multi-objective design optimization, striving for robustness and cost-effectiveness [28]. Applied across industries, FEM ensures high-quality, reliable products under varying conditions [29], promising advancements in transformer design and power systems engineering.

A. Aim and Objectives

This study aims to enhance the resilience of a 50kVA transformer against ferroresonance in low voltage networks by identifying critical design parameters, using the Finite Element Method for optimization. It comprehensively investigates ferroresonance occurrence and effects using MATLAB/Simulink with SimPowerSystems, develops mathematical models for simulation, utilizes the Finite Element Method for optimization, and validates the optimized design through experimental testing.

II. LITERATURE REVIEW

Transformer design optimization plays a crucial role in achieving optimal performance, efficiency, and reliability in power systems. Over the years, researchers and engineers have developed various approaches and techniques to enhance the design of transformers [30]. These approaches include: multi-objective electromagnetic design optimization of power transformers using 3D finite element analysis, response surface methodology, and the third generation non-sorting genetic algorithm [31]; application research based on improved genetic algorithm for optimum design of power transformers [32]; optimization design of high-power high-frequency transformer based on multi-objective genetic algorithm [33]; FEM-based modeling and optimization of dry-type transformers with metaheuristic algorithms [34]; and Split-winding transformer design using new hybrid optimization algorithm based on PSO and Improved Biogeography-Based Binary Cuckoo (I-BB-BC) [19].

ISSN No:-2456-2165 https://doi.org/10.38124/ijisrt/IJISRT24MAY479

Ferroresonance, a complex phenomenon in electrical power systems mainly involving transformers, arises from the interplay between nonlinear characteristics of magnetic cores and system capacitance [1]. This resonance can cause sustained oscillations and generate non-sinusoidal voltage waveforms, posing significant risks to transformer operation and system stability [2][3]. During ferroresonance, transformers may experience abnormal voltage levels and harmonic distortion, inducing increased core losses, heating, and insulation stress, which can compromise performance and lead to catastrophic failure [4][5][6].

Sub-harmonic voltages, occurring as integer fractions of the fundamental frequency, are exacerbated during ferroresonance due to the nonlinear behavior of transformer magnetic cores [7]. These voltages contribute to increased losses and harmonic distortion, underscoring the importance of studying their characteristics and impact for understanding transformer behavior during ferroresonance events [8][9].

Various strategies, including design optimizations and protective measures, are employed to mitigate the adverse effects of ferroresonance and sub-harmonic voltages on transformers [10][11]. Simulation tools like MATLAB/Simulink are employed to model system behavior and validate mitigation strategies [12]. Experimental studies provide valuable insights into transformer behavior under ferroresonance conditions, validating simulation models and refining mitigation strategies [3] [13].

Despite significant research efforts on ferroresonance, challenges and research gaps persist due to limited studies focusing on optimizing transformer cores for inherent resilience against ferroresonance. Computational methods such as Finite Element Analysis (FEA)/Finite Element Method (FEM) offer opportunities to enhance core design by facilitating detailed analysis of transformer performance and optimization techniques [14].

B. Related Works

Various studies explored optimization methods for transformer design to improve efficiency, reliability, and cost-effectiveness in power distribution. [23] optimized transformers using Time-Variant Multi-Objective Particle Swarm Optimization (TV-MOPSO), achieving minor deviations and good results. [15] used cuckoo search for cost reductions and computational efficiency gains. [16] employed mixed-integer programming and finite element methods for cost reduction. [18] proposed a multi-objective methodology using genetic algorithms. [29] utilized particle swarm optimization for noise reduction and cost optimization. [19] proposed a heuristic method for minimal cost compliance with specifications. [34] optimized transformers using FEA and differential evolution for volume and loss reduction. Hashemi et al. (2023) explored heuristic algorithms prioritizing loss reduction. Hernandez et al. (2023) used Non-dominated Sorting Genetic Algorithm III (NSGA-III) for reductions in power losses and weight. [33] compared metaheuristic algorithms for efficiency improvement. [23] employed genetic algorithms for cost reduction and performance improvements. [27] compared evolutionary algorithms for total owning cost reduction. [30] introduced an evolutionary algorithm-based method for conductor shape optimization. [9] optimized shell-type transformers for mass and volume reduction. [29] combined FEM modeling and the Taguchi method for short-circuit impedance reduction.

III. METHODOLOGY

The study involved characterizing the transformer using established models from literature and integrating resulting parameter values into primary and secondary winding configurations, as well as core resistance optimization through parametric analyses. Critical design parameters such as core structure, window dimensions, and winding calculations were meticulously determined; and used in carrying out open and short circuit tests to facilitate design validation using experimental setups. Additionally, the Finite Element Method (FEM) analysis tool within ANSYS Maxwell software was employed for further design optimization and assessment of efficiency under various load conditions. The simulation environment, implemented using MATLAB/Simulink with SimPowerSystems, replicated diverse ferroresonance scenarios in electrical distribution systems, accurately capturing interactions among nonlinear inductances of transformer magnetic cores, characterized non-linear loads, and coupling capacitances. Table 1 presents the parameters of the baseline transformer.

Table 1: Parameters of the Baseline Transformer

Parameter	Value
Rated Power	50kVA
Primary Voltage	11kV
Secondary Voltage	0.415kV
Frequency	50Hz
No-load Loss	340W
Load Loss (75°C)	1174W
Load Loss (120°C)	1230W
No-load Current	2.4%
Short Circuit Impedance	6%
Winding Material (HV/LV)	Copper/Copper

A. The Transformer Analytical Design

The transformer design begins with the selection of an appropriate value of emf/turn. Thus, the equation for emf/turn can be developed by relating the output kVA (Q), the required magnetic and electric loadings (i.e. ϕ_m and AT respectively). A relationship exists between the output equation of the transformer and the emf-per-turn (emf/turn). Thus, the equation for emf/turn can be developed by relating the output kVA (Q), the required magnetic and electric loadings (i.e. ϕ_m and AT respectively). In a transformer, the ratio of the magnetic loading to the electric loading is usually specified rather than an actual value of specific loading. This ratio of the magnetic loading to electric loading is given as:

$$\frac{\phi_m}{AT} = r \quad (1)$$

Where r is a constant.

ISSN No:-2456-2165 https://doi.org/10.38124/ijisrt/IJISRT24MAY479

Now consider the kVA rating of only one phase of the transformer; thus:

$$Q = V_{HV} \times I_{HV} \times 10^{-3} \cong E_{HV} \times I_{HV} \times 10^{-3}$$
$$= (4.44 \times f \times \phi_m \times T_{HV}) \times I_{HV} \times 10^{-3}$$
$$= (4.44 \times f \times \phi_m) \times (I_{HV} \times T_{HV}) \times 10^{-3}$$
$$= (4.44 \times f \times \phi_m) \times (AT_{HV}) \times 10^{-3}$$
$$= (4.44 \times f \times \phi_m) \times \frac{\phi_m}{r} \times 10^{-3} \text{ (using the value of r from eqn (1))}$$
$$= 4.44 \times (\phi_m)^2 \times \left(\frac{f}{r}\right) \times 10^{-3}$$
$$\phi_m = \sqrt{\frac{r \times 10^3}{4.44 \times f}}\left(\sqrt{Q}\right)$$

Voltage per turn,

$$E_t = \frac{E_{HV}}{T_{HV}}$$
$$= \frac{4.44 \times f \times \phi_m \times T_{HV}}{T_{HV}}$$
$$= 4.44 \times f \times \left(\sqrt{\frac{r \times 10^3}{4.44 \times f}}\right)\left(\sqrt{Q}\right)$$
$$= \sqrt{4.44 \times f \times r \times 10^3}\left(\sqrt{Q}\right)$$
$$E_t = K\sqrt{Q} \quad (2)$$

Where $K = \sqrt{4.44 \times f \times r \times 10^3}$ is a constant.

The usual value for different transformer types is listed below:

- Phase shell-type transformers: 1.00 – 1.20
- Phase Core-type transformers: 0.75 – 0.85
- Phase shell-type transformers: 1.30
- Phase Core-type transformers (Distribution): 0.45
- 3-Phase Core-type transformers (Power): 0.60 – 0.70

Once E_t is known, the net cross-sectional area (A_i) of the core can be determined from:

$$A_i = \frac{E_t}{4.44 f B_m} \quad (3)$$

The core area of a transformer is always affected by the weight of the winding conductor as well as the weight of the core itself. Suppose that the area of the core is A_i, weight of copper is G_c and weight of iron core is G_i, then the ratio $(\frac{Weight\ of\ Iron}{Weight\ of\ Copper})$ can be expressed as:

$$\frac{Weight\ of\ Iron}{Weight\ of\ Copper} = \frac{G_i}{G_c} = \frac{A_i l_i g_i}{A_c L_{mc} g_c}$$

Where:
$g_i = specific\ weight\ of\ the\ iron\ core$
$A_i l_i = Total\ volume\ of\ the\ iron\ core$
$g_c = specific\ weight\ of\ the\ copper$
$A_c L_{mc} = Total\ volume\ of\ the\ copper$

And the core area ($A_c = K_w A_w$); where; A_w is the core window area and K_w is the window space factor; given as $K_w = \frac{Total\ Copper\ Area\ in\ Window}{Total\ Window\ Area} = \frac{A_c}{A_w}$. So that:

$$\frac{G_i}{G_c} = \frac{A_i l_i g_i}{K_w A_w L_{mc} g_c} \quad (4)$$

Making $K_w A_w$ subject of the expression in equation (3):

$$K_w A_w = \left(\frac{G_c}{G_i}\right)\left(\frac{A_i l_i g_i}{L_{mc} g_c}\right) = \left(\frac{l_i g_i}{L_{mc} g_c}\right)\left(\frac{G_c A_i}{G_i}\right)$$

If we assume $\frac{l_i g_i}{L_{mc} g_c}$ to be a constant (K_1), then:

$$K_w A_w = K_1\left(\frac{G_c A_i}{G_i}\right) \quad (5)$$

Recalling that the output equation of a transformer can be expressed as:

$$Q = 3.33 f B_m A_i K_w A_w \delta \times 10^3 \quad (6)$$

Then substituting equation (5) into equation (6), we have:

$$Q = 3.33 f B_m A_i K_1\left(\frac{G_c A_i}{G_i}\right)\delta \times 10^3$$
$$= 3.33 f B_m A_i^2 K_1 \frac{G_c}{G_i}\delta \times 10^3$$

Therefore:

$$A_i^2 = \frac{Q}{3.33 f B_m K_1 \frac{G_c}{G_i}\delta \times 10^3}$$
$$A_i = \sqrt{\frac{10^3}{3.33 K_1}\frac{Q}{f B_m \delta}\frac{G_i}{G_c}} \quad (7)$$

Equation (7) is an expression for the total iron core area.

The total area of the copper winding can also be expressed in terms of the HV and LV ampere-turns (AT) of the distribution transformer. Thus:

$$A_i = 2[(T_{HV} \times a_{HV}) + (T_{LV} \times a_{LV})]$$
$$= 2\left[\left(T_{HV} \times \left(\frac{I_{HV}}{\delta}\right)\right) + \left(T_{LV} \times \left(\frac{I_{LV}}{\delta}\right)\right)\right]$$
$$= \frac{2}{\delta}[(T_{HV} \times I_{HV}) + (T_{LV} \times I_{LV})]$$
$$= \frac{2}{\delta}[(mmf\ of\ HV\ winding) + (mmf\ of\ LV\ winding)]$$

ISSN No:-2456-2165 https://doi.org/10.38124/ijisrt/IJISRT24MAY479

$$= \frac{2}{\delta}[(AT) + (AT)]$$

$$\therefore A_c = \frac{4}{\delta}[AT] \quad (8)$$

Now, it is known that Window Space Factor (K_W) is given as:

$$K_W = \frac{A_c}{A_w} \quad (9)$$

Then equation substituting for A_c from equation (8) in equation (9);

$$K_W = \frac{\frac{4}{\delta}[AT]}{A_w}$$

So that;

$$AT = \frac{K_W A_w \delta}{4} \quad (10)$$

The rating of a distribution tranformer can generally be expressed as:

$$Q = 3 \times V_{HV} \times I_{HV} \times 10^{-3} \quad (11)$$

Equation (11) can also be represented as:

$$Q = 3 \times E_{HV} \times I_{HV} \times 10^{-3} \quad (12)$$
$$= 3 \times (4.44 \times f \times \phi_m \times T_{HV}) \times I_{HV} \times 10^{-3}$$
$$= 3 \times (4.44 \times f \times \phi_m) \times (I_{HV} \times T_{HV}) \times 10^{-3}$$
$$= 3 \times (4.44 \times f \times \phi_m) \times (AT_{HV}) \times 10^{-3}$$

Since $AT = \frac{K_W A_w \delta}{4}$, then:

$$= 3 \times (4.44 \times f \times \phi_m) \times \left(\frac{K_W A_w \delta}{4}\right) \times 10^{-3}$$

So that:

$$Q = 3 \times \left(1.11 \times f(B_m \times A_i)\right) \times (K_W A_w \delta) \times 10^{-3}$$

$$Q = 3.33 f B_m A_i K_W A_w \delta \times 10^{-3} \text{ (back to equation (6))}$$

This transformer output equation; as evidenced in equation (6) is applicable to both core type and shell type transformers; and is used in optimizing the design for minimum loss, cost, weight and size. Most times the Window Space Factor (K_w) can also be expressed as:

$$K_w = \frac{2}{\left(\frac{30}{kV}\right) + 8} \quad (13)$$

Where (kV) is the kVA rating of the transformer.

B. Core Design Optimization

To optimize the transformer core design, Finite Element Method (FEM) was utilized for extensive parametric sweep analyses, aimed at maximizing efficiency. Various parameters, including output power (Q, in kVA), maximum flux in the core (ϕ_m, in Wb), supply frequency (f, in Hz), and maximum flux density (B_m, in Wb/m^2), were evaluated. A constant value (K) of 0.45 was chosen for distribution transformers to ensure consistency. The objective was to identify the design configuration that achieves the optimal balance between performance and cost, ensuring the transformer meets desired specifications effectively and economically.

For this analysis, M6 Steel was selected as the core material, accompanied by a suitably sized 6-stepped core design. The voltage per turn (E_t, in V) was calculated using equation (2). Additionally, parameters such as maximum flux in the core, net iron area (A_i), and width of the laminations ($W_{Laminations}$) were determined using the provided equations (3 through 13). Finally, increasing the core resistance at the core design stage was achieved through the following approach during the FEM optimization (as illustrated in Figures 2 and 3):

- **Material Selection**: M6-Core material with higher resistivity was chosen to naturally increase the core resistance. Utilizing a material with higher silicon content in silicon steel laminations was prioritized to elevate resistivity and hence core resistance.
- **Core Coatings**: Application of coatings or surface treatments to the core material was implemented to enhance resistance. These coatings aided in reducing eddy current losses, thereby increasing the effective resistance of the core.
- **Interleaved or Segmented Cores**: Designing the core with interleaved or segmented laminations introduced additional resistance at the interfaces between the laminations, effectively boosting the overall core resistance.
- **Core Shape and Geometry**: Modification of the shape and geometry of the core was undertaken to impact resistance. Employing thinner laminations or increasing the length-to-diameter ratio of the core was explored to alter the magnetic flux distribution and elevate resistance.
- **Gap Adjustments**: Introduction of controlled air gaps in the core was used to increase resistance by reducing the effective permeability of the core material. This helped in controlling saturation levels and reducing losses.
- **Temperature Effects**: Consideration of temperature effects on core resistance was deemed crucial. Core resistance typically increases with temperature, so designing for higher operating temperatures was embraced to naturally increase core resistance.
- **Material Processing**: Various processing techniques, such as annealing or stress relief, were utilized to alter the microstructure of the core material, affecting its resistivity and hence core resistance.

While increasing core resistance, careful attention was given to its impact on other performance parameters, such as efficiency, losses, and magnetic characteristics. Balancing these factors ensured that the transformer met its design requirements while effectively mitigating ferroresonance

ISSN No:-2456-2165 https://doi.org/10.38124/ijisrt/IJISRT24MAY479

effects. Now, let's consider the impact of introducing a resistive load (in the form of a predetermined core resistance R_{fe}) to the circuit through the process just described above. The equivalent circuit representing this situation is depicted in Figure 1.

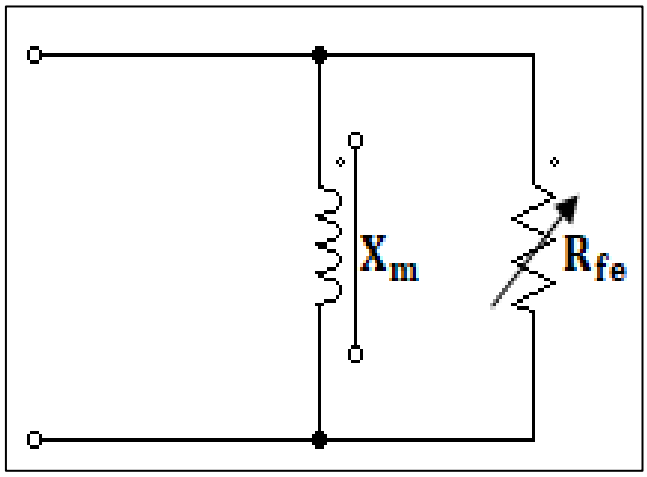

Fig 1: Equivalent Transformer Circuit with Resistive Load [14]

The series equivalent impedance can be calculated using the formula:

$$Z_{eq} = \frac{(jX_m)(R_L)}{(R_{fe} + jX_m)} \quad (14)$$

Multiplying top and bottom by $R_L - jX_m$,

$$Z_{eq} = \frac{(jX_m R_L)(R_{fe} - jX_m)}{({R_{fe}}^2 + {X_m}^2)} \quad (15)$$

Simplifying:

$$Z_{eq} = \frac{{X_m}^2 R_{fe}}{{R_{fe}}^2 + {X_m}^2} + j\frac{X_m {R_{fe}}^2}{{R_{fe}}^2 + {X_m}^2} \quad (16)$$

Thus, the term $\frac{{X_m}^2 R_{fe}}{{R_{fe}}^2 + {X_m}^2}$ represents an added series resistance in the ferroresonant circuit. Its effect will be to significantly shorten the ellipse of composite operating points; and thereby reduce the worst case magnitudes of both voltage and current. It is for this reason that resistive loading is a proven technique for controlling ferroresonance. When R_L approaches infinity, simulating a no-load condition, the value of this term can be determined using L'Hospital's Rule.

$$\lim_{R_{fe}\to\infty} \frac{{X_m}^2 R_{fe}}{{R_{fe}}^2 + {X_m}^2} = \lim \frac{{X_m}^2}{2R_{fe}} = 0 \quad (17)$$

This implies that the series resistance term diminishes and eventually vanishes as the transformer loading decreases. The inductive term experiences a similar alteration.

$$\lim_{R_{fe}\to\infty} \frac{{X_m}^2 R_{fe}}{{R_{fe}}^2 + {X_m}^2} = \lim \frac{2X_m R_{fe}}{2R_{fe}} = X_m \quad (18)$$

So that, under no-load conditions, the total transformer impedance reduces to X_m. By designing the transformer core so that R_{fe} is large enough, the transformer can be optimized to withstand extreme ferroresonance conditions long enough for system ancillaries to detect the contingencies and initiate necessary containment measures.

A. Estimation of Design Parameters for the Core

- *Emf per turn (E_t):*

Formula used:
$E_t = K\sqrt{Q}$

Where $K = \sqrt{4.44 \times f \times r \times 10^3}$ is a constant.

Calculation:

$E_t = 0.5\sqrt{50} = 3.535V$

- *Maximum flux (ϕ_m):*

Formula used:
$\phi_m = \frac{E_t}{4.44f}$

Calculation:

$\phi_m = \frac{3.535}{4.44f} = \frac{3.535}{4.44 \times 50} = \frac{3.535}{222} = 15.926 \times 10^{-3} Wb$

- *Net Iron Area (A_i):*

Formula used:

$A_i = \frac{\phi_m}{B_m}$

Calculation:

$A_i = \frac{15.926 \times 10^{-3}}{1.44} = 11.1 \times 10^{-3}(m^2)(\times 10^6) = 11.1 \times 10^3 mm^2$

- *Core Structure:*

Formula used:

$A_i = kd^2, so\ that\ d = \sqrt{\frac{A_i}{K}}$

Calculation:

$d = \sqrt{\frac{11.1 \times 10^3}{0.65}} = 136.68mm$

ISSN No:-2456-2165 https://doi.org/10.38124/ijisrt/IJISRT24MAY479

➢ *Laminated Core Width:*

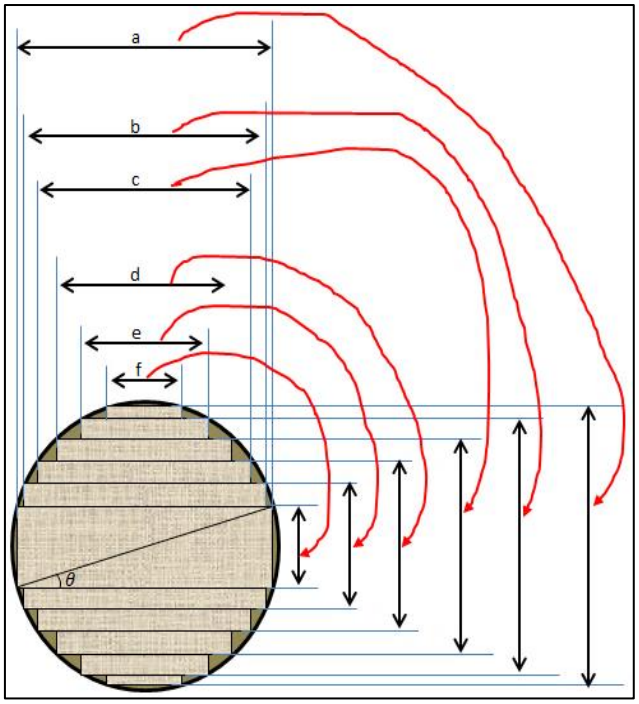

Fig 2: The Optimized 6-Stepped Core Design

Now a 6-stepped core design (Figure 2) would have stacks a, b, c, d, e, and f of laminated sheets. So each stack would have the width as follows:

$a = 0.96 \times 136.68 = 131.21mm$
$b = 0.88 \times 136.68 = 120.28mm$
$c = 0.77 \times 136.68 = 105.24mm$
$d = 0.64 \times 136.68 = 87.48mm$
$e = 0.48 \times 136.68 = 65.61mm$
$f = 0.28 \times 136.68 = 38.27mm$

➢ *Total Core Width (W_w):*

Formula used:

$W_w = a(i.e. width\ of\ the\ largest\ stamping)$

Calculation:

$W_w = a = 0.96 \times 136.68 = 131.21mm$

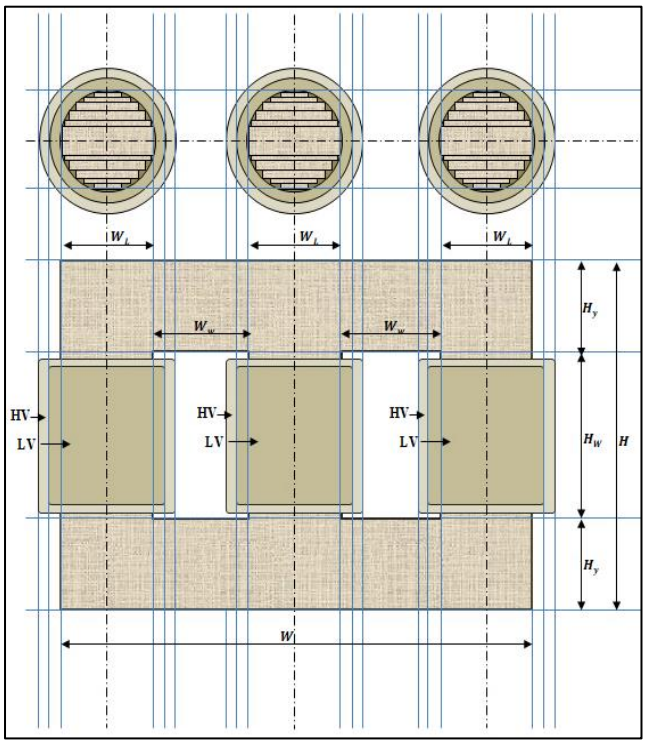

Fig 3: Overall Details of the Core

➢ *Window Dimensions:*

Formula used:

Now assuming that Height of the yoke H_y = (1.5)a, and the Height of the window (H_w) is 3 times the window width (W_w), then:

$H_y = (1.5) \times 131.21 = 196.82mm$

And;

$H_w = 3W_w = 3 \times 131.21 = 393.63mm$

Then;

$Window\ Area\ (A_w) = H_w W_w = 3W_w^2 = 3 \times (131.21)^2 = 17.22 \times 10^3 mm^2$

Thus;

Overall Length (W) of the transformer core $= 2W_w + d + 3a$

$W = 2(131.21) + 136.68 + 3(131.21) = 792.73mm$

So that;

Overall Height (H)of the transformer core $= 2H_y + H_w$

$H = 2(196.82) + 393.63 = 787.27mm$

Graphical details of the core dimensions are illustrated by Figure 3.

ISSN No:-2456-2165 https://doi.org/10.38124/ijisrt/IJISRT24MAY479

B. Estimation of Winding Parameters

Number of primary turns (N_P) would be given as:

$$N_P = \frac{V_P}{E_t} = \frac{11000}{3.535} = 3000turns$$

And number of secondary turns (N_S) would be given as:

$$N_S = \frac{V_S}{E_t} = \frac{415}{3.535} = 117turns$$

The primary current (I_P) would then be:

$$I_P = \frac{kVA \times 10^3}{V_P} = \frac{50 \times 10^3}{11 \times 10^3} = 4.55Amps$$

So that the C.S.A. of the primary winding conductor (a_P) would be:

$$a_P = \frac{\text{The primary current } (I_P)}{Maximum\ Current\ Density\ (\delta)} = \frac{4.55}{2.5} = 1.82 \cong 2mm^2$$

The secondary current (I_S) would be given as:

$$I_S = \frac{kVA \times 10^3}{V_S} = \frac{50 \times 10^3}{415} = 120.48 \cong 120.5Amps$$

So that the C.S.A. of the secondary winding conductor (a_S) would be:

$$a_S = \frac{\text{The primary current } (I_S)}{Maximum\ Current\ Density\ (\delta)} = \frac{120.5}{2.5} = 48.2 \cong 50mm^2$$

C. Modeling the Distribution System under Ferroresonance Conditions

Ferroresonance is modelled as a nonlinear inductor (L_{NL}) alongside linear elements; R, L, and C as illustrated in Figure 4.

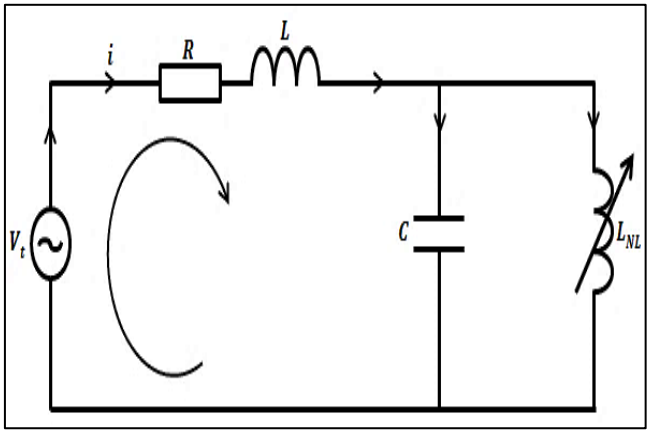

Fig 4: Equivalent Circuit of AC Distribution System under Ferroresonance Condition [1]

Thus, the total voltage in the system (V_t); during a ferroresonant event; and expressed as a summation of multiple sinusoidal terms would be given by:

$$V_t = V_1 + \sum n\left(V_n\, cos(n\omega t + \varphi_n)\right) \quad (19)$$

Where:

V_1 is the fundamental voltage component with angular frequency ωt and phase angle φ_1. The summation term ($\sum n$) includes higher-order harmonics ($n > 1$) with respective amplitudes V_n and phase angles φ_n. These higher-order harmonics account for the distortion or non-sinusoidal behavior in the voltage waveform during transient events. Then, the total current in the system (I_t); also expressed as a summation of multiple sinusoidal terms during the ferroresonant event would be given by:

$$I_t = I_1 + \sum n\left(I_n \cos(n\omega t + \theta_n)\right) \quad (20)$$

Where:

I_1 is the fundamental current component with angular frequency ωt and phase angle θ_1. The summation term ($\sum n$) includes higher-order harmonics ($n > 1$) with respective amplitudes I_n and phase angles θ_n. These higher-order harmonics account for the distortion or non-sinusoidal behavior in the current waveform during transient events.

It will be assumed that the distribution network includes linear elements like resistance (R) and inductance (L) and nonlinear elements like capacitance (C) and nonlinear inductance (V_{NL}).

From Kirchhoff's Voltage Law (KVL), the total voltage applied to the network is the sum of all the voltage drops across the network elements; namely; the voltage drop across the resistance (V_R), the voltage drop across the linear inductance (V_L), the voltage drop across the nonlinear capacitance (V_C), and the voltage drop across the nonlinear inductance (V_{NL}). Thus:

$$V_t = V_R + V_L + V_C + V_{NL} \quad (21)$$

Where

$V_R = iR;$

$V_L = L\frac{di}{dt};$

$V_C = \frac{1}{C}\int i(t)dt$

$V_{NL} = L_{NL}i^2 \cdot \frac{d(i^2)}{dt}$

So that:

ISSN No:-2456-2165 https://doi.org/10.38124/ijisrt/IJISRT24MAY479

$$V_t = V + \sum n\left(V_n \cos(n\omega t + \varphi_n)\right) = i(t)R + L\frac{di}{dt} + \frac{1}{C}\int i(t)dt + L_{NL}i^2 \cdot \frac{d(i^2)}{dt} \quad (22)$$

Suppose that the current in the network is given by:

$$i(t) = I_1 + \sum n\,(I_n \cos(n\omega t + \theta_n) \quad (23)$$

Then, substituting the expression for i(t) into KVL equation (15); and expanding:

$$V + \sum n\left(V_n \cos(n\omega t + \varphi_n)\right) = (I_1 R) + \sum n\,(I_n R\cos(n\omega t + \theta_n)) + L\frac{d(I_1)}{dt}$$

$$V_t = V + \left[I_1 + \sum n\left(I_n\cos(n\omega t + \theta_n)\right)\right]R + L\frac{d}{dt}\left[I_1 + \sum n\left(I_n\cos(n\omega t + \theta_n)\right)\right] + \frac{1}{C}\int\left[I_1 + \sum n\left(I_n\cos(n\omega t + \theta_n)\right)\right] + L_N L\frac{d\left\{\left[I_1 + \sum n\left(I_n\cos(n\omega t + \theta_n)\right)\right]^2\right\}}{dt} \quad (24)$$

The derivative of the cosine term can be simplified using the chain rule:

$$\frac{d(\cos(n\omega t + \theta_n)}{dt} = -n\omega \times \sin(n\omega t + \theta_n) \quad (25)$$

After integrating and differentiating:

$$V + \sum n\left(V_n\cos(n\omega t + \varphi_n)\right) = (I_1 R) + \sum n\left(I_n R\cos(n\omega t + \theta_n)\right)$$

$$+L\frac{d(I_1)}{dt} - \sum n\left(n\omega L I_n \sin(n\omega t + \theta_n)\right) + \left(\frac{1}{C}\right) \times \left(I_1 t + \sum n\left(I_n\left(\frac{1}{n\omega}\right)\sin(n\omega t + \theta_n\right)\right.$$

$$+L_{NL}\left(I_1^2 + 2I_1\sum n(I_n\cos(n\omega t + \theta_n))\right) + \sum n(I_n^2\cos^2(n\omega t + \theta_n)) \times 2\,I_1\frac{d(I_1)}{dt}$$

$$+2\sum n\,(I_n\cos(n\omega t + \theta_n))\frac{d(I_n)}{dt} \quad (26)$$

The coefficients (I_1, I_n, V_n, θ_n, φ_n) will depend on the particular network configuration and the behavior of the nonlinear elements. The nonlinear inductance term (L_{NL}) represents the contribution of the nonlinear inductance to the overall system behavior.

- **Assumptions**: A single harmonic component ($n = 1$) was considered for both voltage and current. This means we assume only one frequency (ω) is present in the system, and the other harmonic components are negligible. The nonlinear inductance term (L_{NL}) is constant and can be represented by a single parameter (L_{NL}).

➢ *With these Assumptions, the Equation Becomes:*

$$V_t = V + V_1\cos(\omega t + \varphi_1) = I_1 R + L\frac{d(I_1)}{dt} + \left(\frac{1}{C}\right)\int I_1 dt + L_{NL}I_1^2\frac{d(I_1^2)}{dt} \quad (27)$$

So that for 'n' number of harmonics:

$$V_t = V + \sum n\left(V_n\cos(n\omega t + \varphi_n)\right) = iR + L\frac{di}{dt} + \frac{1}{C}\int i(t)dt + L_{NL}i^2 \cdot \frac{d(i^2)}{dt} \quad (28)$$

The model aids in simulating network behavior across various operational scenarios and pinpointing potential ferroresonance triggers, including resonant frequencies, switching events, nonlinear loads, faults, and transformer configurations, enabling proactive identification and mitigation of ferroresonance risks.

D. Modeling of the Passive Nonlinear Elements within the Distribution System

For the characterization of magnetic behavior and its impact on system dynamics, equations (29) through (17) are developed:

$$b = F_1\left(h, \frac{dh}{dt}, \ldots, \frac{db}{dt}, \frac{d^2b}{dt^2}, \ldots\right) \quad (29)$$

In practical scenarios, the current (i) in a nonlinear inductance (NI) often depends on the flux linkage (ψ). In such cases, neglecting higher-order derivatives, equation (29) can be simplified to the following form:

$$i = F_2\left(\psi, \psi^n; \frac{d\psi}{dt}, \frac{d^2\psi}{dt^2}\ldots\right) \quad (30)$$

ISSN No:-2456-2165 https://doi.org/10.38124/ijisrt/IJISRT24MAY479

Equation (30) in the general case describes the equivalent circuit of the Nonlinear Inductances, which is its generalized model as illustrated in Figure 5.

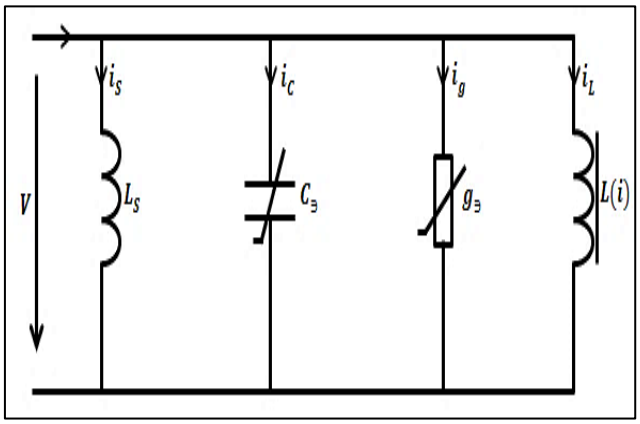

Fig 5: Generalized Nonlinear Inductance Electromagnetic Transformer (NI-EMT) Model [1]

Assuming that the equivalent parameters L_s (leakage inductances in the system; such as transformers), $C_э$ (system capacitances), and $g_э$ (equivalent active conductivity of the system representing all resistance elements in the distribution system that account for the damping effect within the system) in this circuit are constant, then we obtain equation (31):

$$i = C_э\frac{d^2\psi}{dt^2} + g_э\frac{d\psi}{dt}a\psi + b\psi^n + \frac{\psi}{L_S} \tag{31}$$

Where $b\psi^n$ is the approximation of the Weber-ampere characteristic of the system, obtained on the basis of the magnetization curve $B = f(H)$, $C_э$is the equivalent electromagnetic (coupling) capacitance of the system, $g_э$is the equivalent active conductivity of the system; $L_S$is the leakage inductance of the system. Assuming that the voltage across the inductor is described by $v = V_m \cos \omega t$, Then:

$$\begin{cases} i_S = \dfrac{\psi}{L_S} = a\psi;\ 2nd\ derivative\ of\ a = \dfrac{1}{L_S}; \\ \psi = \dfrac{V_m}{\omega}\sin\omega t = \Psi_m \sin\omega t; \\ i_C = C_э\dfrac{d^2\psi}{dt^2} = -\omega^2 C_э \Psi_m \sin\omega t = -I_{Cm}\sin\omega t; \\ i_g = \dfrac{1}{R_э}\cdot\dfrac{d\psi}{dt} = \dfrac{\Psi_m\omega}{R_э}\cos\omega t = I_{gm}\cos\omega t. \end{cases} \tag{32}$$

From (31), taking into account the adopted approximation, it then follows that:

$$\begin{cases} i_C = \dfrac{I_{cm}}{\Psi_m}\psi; \\ i_g = \pm\dfrac{I_{gm}}{\Psi_m}\sqrt{\Psi_m^2 - \psi^2}; \\ i_L = a\psi + b\psi^n, \end{cases} \tag{33}$$

Where $i_L' = i_S + i_L$. Thus from (31):

$$i = \left(a - \frac{I_{cm}}{\Psi_m}\right)\psi + b\psi^n \pm \frac{I_{gm}}{\Psi_m}\sqrt{\Psi_m^2 - \psi^2} \tag{34}$$

The analysis of ferroresonance in the low voltage distribution system transformer was performed by modifying the equivalent circuit of Figure 3 with distribution transformer (Electro-Magnetic Transformers or EMTs) and network capacitances using the generalized model of nonlinear inductance (NI).

Assuming that Σ_g, Σ_C and L_0account for all existing system nonlinear components, then equation (31) can be approximated thus:

$$i = \sum C\frac{d^2}{dt^2} + \sum g\frac{d\psi}{dt} + a\psi + b\psi^n + \frac{\psi}{L_0} \tag{35}$$

Where $\sum C$ represents the total electromagnetic capacitance of the distribution transformer, $\sum g = \frac{1}{\sum R}$is the equivalent active conductivity of the system (representing all resistance elements in the transformer that account for the damping effect within the system), L_0represents the equivalent leakage inductances (representing all the nonlinear inductive circuits within the system) and $a\psi + b\psi^n = i_{\mu H}$ is the approximation of Wb-Amp characteristics of the system.

Equation (35) is used to describe a modification of the equivalent circuit of Figure 4; as illustrated by Figure 6.

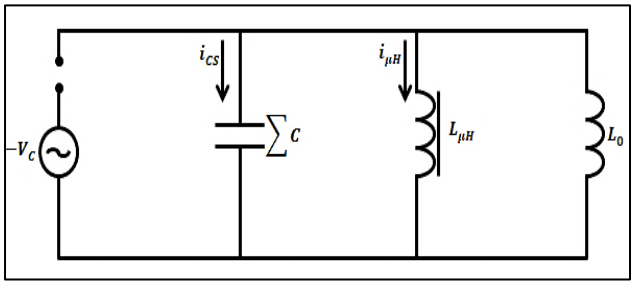

Fig 6: Equivalent Circuit of the Studied Transformer with Nonlinear Inductances (Distribution Transformers and Other System Inductances), Resistive Loads and Capacitances [1]

Considering that the voltage in Figure 5 is $v = V_m \cos\omega t$, and taking into account the [25] adopted approximation of the Weber-ampere characteristic of NI EMT model:

$$\begin{cases} i\sum C = \dfrac{I_{cm}}{\Psi_m}\psi; \\ i\sum g = \pm\dfrac{I_{gm}}{\Psi_m}\sqrt{\Psi_m^2 - \psi^2}; \\ i_{\mu H} = a\psi + b\psi^n, \end{cases} \tag{36}$$

ISSN No:-2456-2165 https://doi.org/10.38124/ijisrt/IJISRT24MAY479

From (36), we obtain:

$$i = i_{\sum C} + i_{\sum g} + i_{\mu H} = \left(a - \frac{I_{cm}}{\Psi_m}\right)\psi + b\psi^n \pm \frac{I_{gm}}{\Psi_m}\sqrt{\Psi_m^2 - \psi^2} \quad (37)$$

Equation (37) presents the dynamic characteristic of distribution transformer similar to the hysteresis loop of nonlinear inductance, influenced by the dynamic coercive force (H_{cd}) and time-varying magnetic induction ($B = B_m \sin \omega t$) in the core, critical for the transformer current conduction efficiency. Thus:

$$H_{cd} = H_C 0.125\omega\sigma d^2 B_S\sqrt{2\varepsilon - 1} \quad (38)$$

The Dynamic Coercive Force (H_{cd}) represents the magnetic field strength necessary to demagnetize the core material during dynamic magnetization, signifying the point at which ferromagnetic material loses its magnetization and serves as a critical parameter in the core material's behavior.

Magnetic Core Material (μ_f) is the material used for the core of the transformer, typically made of ferromagnetic material like iron or silicon steel. The choice of core material influences the magnetic properties and behavior of the transformer, including its ability to sustain magnetization.

Induction (in this context, $B = B_m \sin(\omega t)$) represents the time-varying magnetic induction (B) in the core of the transformer. It is expressed as a sinusoidal function of time ($\sin(\omega t)$), where "B_m" represents the peak magnetic induction and "ω" represents the angular frequency of the alternating current.

- H_C is the static coercive force, representing the magnetic field strength required to reduce the magnetic induction (B) to zero under static conditions.
- ω is the angular frequency of the alternating current (AC) flowing through the transformer.
- d is the thickness of the ferromagnetic material, which is used to construct the core of the transformer.
- σ is the conductivity of the core material expressed as ($\sigma = \frac{B_m}{B_S}$).
- B_S is the saturation magnetic induction, representing the maximum magnetic induction that the core material can sustain under given operating conditions.
- ε is the coefficient of the dynamic hysteresis loop, representing the dynamic behavior of the ferromagnetic material during magnetization.

The dynamic coercive force (H_{cd}) accounts for the effects of both static and dynamic magnetization processes in the core material of the transformer. It reflects the combined influence of the static coercive force (H_C) and the dynamic behavior characterized by the term ($0.125\omega\sigma d^2 B_S\sqrt{2\varepsilon - 1}$). This term takes into account the thickness of the core material (d), the material conductivity (σ) of the core, the angular frequency of the alternating current (AC) signal (ω), the saturation magnetic induction (B_S), and the coefficient of the dynamic hysteresis loop (ε). These factors collectively contribute to the ability of the core material to sustain magnetization and play a crucial role in determining the performance and behavior of the transformer during operation.

The dynamic coercive force (H_{cd}), is therefore, critical factor in modeling the behavior of the transformer core material, particularly in scenarios involving alternating magnetization, such as those to be simulated for the studied transformer under normal and ferroresonant conditions.

If 'V' is the voltage applied to the transformer, and '$\sum R$' the total resistance in the circuit, then:

$$\frac{V}{\sum R} = \frac{H_{cdl}}{w} = \frac{l}{w}\left(H_C + 0.125\omega\sigma d^2 B_S\sqrt{2\varepsilon - 1}\right) \quad (39)$$

Where *l*; is the length of the core, and; the term $\frac{l}{w}$ refers to the ratio of the length (l) of the core to the width (w) of the core. This ratio is used here to represent the geometric factor in respect of the core, H_{cdl} is the effective permeability of the magnetic core under the influence of ferroresonance. To get the equivalent active resistance of the nonlinear electromagnetic transformer (NI EMT) voltage:

$$\sum R = \frac{Vw}{l\left(H_C + 0.125\omega\sigma d^2 B_S\sqrt{2\varepsilon - 1}\right)} = \frac{\omega w^2 SB}{l\left(H_C + 0.125\omega\sigma d^2 B_S\sqrt{2\varepsilon - 1}\right)} \quad (40)$$

Where 'w' is the width of the core; 'S' is the cross-sectional area of the magnetic core. It is a measure of the area perpendicular to the direction of magnetic flux; and 'B' represents the magnetic induction or magnetic flux density in the magnetic core.

Using equation (36) the equivalent parameters $\sum C$ and L_0 for the transformer were determined thus:

$$\sum C = \frac{a\Psi_r + b\Psi_r^n - \frac{1}{R}\sqrt{(V_m^2 - \Psi_r^2\omega^2)}}{\omega^2\psi_r} = \frac{a\Psi_r + b\Psi_r^n - \frac{\omega}{R}\sqrt{(\Psi_m^2 - \Psi_r^2)}}{\omega^2\psi_r} \quad (41)$$

ISSN No:-2456-2165 https://doi.org/10.38124/ijisrt/IJISRT24MAY479

And;

$$L_0 = \frac{\psi_r}{\frac{1}{\psi_m}\left(I_{cm}\psi_r + I_{gm}\sqrt{\psi_m^2 - \psi_r^2}\right) - b\psi_r^n} \quad (42)$$

Let's define an expression for instantaneous values of current and active power in the system. Considering that the flux linkage in the dynamic characteristic of NI EMT is given by $\psi = \psi_m \sin \omega t$; and taking into account that $i_{\mu H} = a\psi + b\psi^n$, then for the current in the ascending branch of the hysteresis loop, the following expression holds:

$$i = I_{1m} \sin(\omega t + a) - \frac{b}{4}\Psi_m^n \sin 3\omega t \quad (43)$$

Where:
I_{1m} is the maximum value of the current in the ascending branch of the hysteresis loop.
a is a phase angle related to the system parameters (I_{gm}, $a\Psi_m + (\frac{3}{4})\,b\Psi_m^n - I_{cm}$).
b is a coefficient related to the nonlinear behavior of the system.
Ψ_m^n is the nth power of the maximum magnetic flux linkage ψ_m.

And:

$$I_{1M} = \sqrt{\left(a\Psi_m + \frac{3}{4}b\Psi_m^n - I_{cm}\right)^2 + I_{gm}^2} \quad (44)$$

Where:
I_{gm} is the amplitude of the Gauss random noise in the system.
I_{cm} is the minimum value of the current in the descending branch of the hysteresis loop.

And:

$$a = arctg\frac{I_{gm}}{a\Psi_m + \frac{3}{4}b\Psi_m^n - I_{cm}} \quad (45)$$

If the instantaneous power in the nonlinear transformer equals:

$$p = V_m I_{1m} \cos\omega t \sin(\omega t + a) - \frac{b}{4}V_m\Psi_m^n; \quad (46)$$

Then the core loss becomes:

$$p_{Loss} = \frac{w^2S^2\omega^2B_m^2}{2} \cdot \frac{1}{\sum R} = 2\pi^2 w^2 S^2 f^2 \sigma B_m^2 \quad (47)$$

Where:

$$\sum \sigma = \frac{1}{\sum R} \quad (48)$$

On the basis of equations(34) through (48), various magnetic characteristics can be realized for the core material of the studied transformer.

E. No-Load Losses Formulation based on Finite Element Method (FEM)

Using FEM, the validation computes no-load losses of the optimized transformer under varied conditions. This approach assesses efficiency considering anisotropy, non-linearity, voltage boundary, directionality of losses, joints, air gaps, and stacking holes. The main equation is the magneto-static Maxwell equation reported by [15]:

$$\nabla \times = 0 \nabla \times B = 0 \quad (49)$$

Where B is the magnetic flux density vector and r is the reluctivity tensor. When analyzing induction machines, particularly under AC excitation, the air gap's magnetic field becomes dynamically changing. In materials exhibiting non-zero conductivity, eddy currents are induced. Consequently, this alters the nature of the field problem depicted by equation (49), transforming it into a magneto-dynamic scenario characterized by nonlinearity and time-harmonic behavior represented by equation (50).

$$\bar{V} \times \left(\frac{1}{\mu B}\bar{V} \times A\right) = -\sigma A + J_{src} - \sigma \nabla V \quad (50)$$

The equation presented captures this transformation, depicting the intricate interplay between voltage (V), magnetic flux density (B), magnetic vector potential (A), conductivity (σ), current density (J_{src}), and voltage gradient (∇V). A common model for the reluctivity tensor is given by:

$$r = \begin{bmatrix} r_{xx} & 0 & 0 \\ 0 & r_{yy} & 0 \\ 0 & 0 & r_{zz} \end{bmatrix} \quad (51)$$

The elements r_{xx}, r_{yy}, and r_{zz} are highly non-linear functions of the magnetic flux density B. Although the non-diagonal elements of the reluctivity tensor are affected by the core material's crystalline structure, we simplify modeling for efficiency. Gaussian curve fitting with three terms captures the non-linear behavior of relative permeability elements as seen in equation (52).

$$\frac{1}{r\mu_0} = \mu_r = a_1 e^{-\left(\frac{B-b_1}{c_1}\right)^2} + a_1 e^{-\left(\frac{B-b_2}{c_2}\right)^2} + a_1 e^{-\left(\frac{B-b_3}{c_3}\right)^2} + 1 \quad (52)$$

Here, μ_0 represents vacuum permeability, and μ_r denotes relative permeability. The parameters a_i, b_i, and c_i are determined using a curve fitting algorithm.

Equation (53) computes transformer core losses as proposed by [16,17]:

ISSN No:-2456-2165 https://doi.org/10.38124/ijisrt/IJISRT24MAY479

$$P = K_h B_M^{(n_a B_m^2 + n_b B_m + n_c)} + \frac{1}{T}\int_{t=0}^{T} \frac{\sigma a^2}{12\rho}\left|\frac{dB}{dt}\right|^2 dt + \frac{1}{T}\int_{t=0}^{T} K_{exc}\frac{\sigma a^2}{12\rho}\left|\frac{dB}{dt}\right|^{1.5} dt \quad (53)$$

Where B_m is the maximum flux density, a, σ, ρ, and T represent sheet thickness, conductivity, mass density, and time period respectively. K_h, K_{exc}, and n are constant coefficients derived from sheet loss data at specific frequencies and flux densities. Figure 7 illustrates the routine flowchart employed in conducting finite element analysis for the analyzed transformer.

The FEM approach utilized in this study consisted of three phases: pre-processing, processing, and post-processing. In pre-processing, object geometry and boundary conditions are defined, including Dirichlet boundary conditions to constrain magnetic flux. Processing involved analyzing system behavior based on these conditions and material properties, considering applied loads.

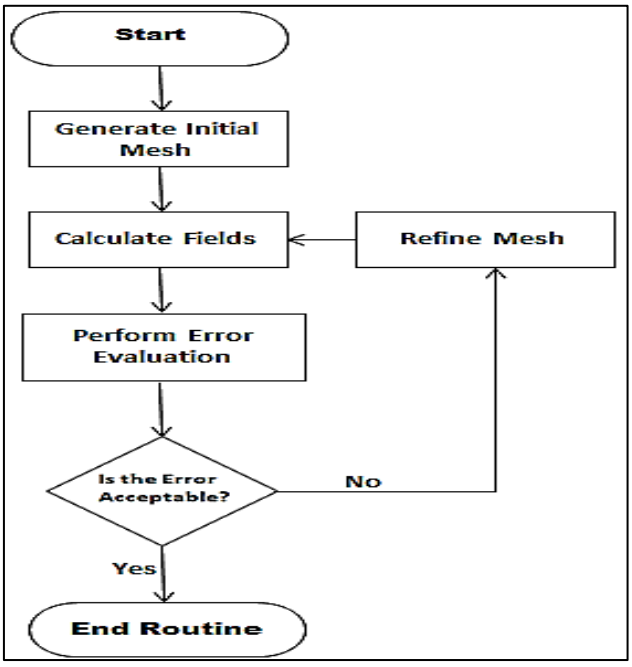

Fig 7: Algorithm Flowchart for the FEM Implementation

Post-processing examined analysis results, visualizing physical quantities like stress and electromagnetic fields. Material properties, such as magnetization function and permeability, are input, allowing for nonlinearity and inclusion of hysteresis effects. Through the discretization of the core geometry and subsequent solution of Maxwell's equations, the simulation captured intricate electromagnetic behaviors, accounting for core losses attributed to eddy currents and hysteresis.

F. FEM Modeling and Simulation Set-up

The FEM finite element model is realized by first defining the geometry of the problem domain, including boundaries, surfaces and volumes. By discretizing the transformer core geometry and solving equations (45) through (48) numerically, the complex electromagnetic phenomena within the transformer core were simulated accordingly. The clamp, pad, and base were omitted due to their negligible influence on the leakage magnetic field. Only the structural models of the core, winding, and insulation are considered. The iron core is treated as a single entity, with negligible interaction between its silicon steel sheets, and the winding shape is simplified into a cylinder. Meshing operations realized a finite element mesh with 713,228 nodes and 1,206,620 elements, ensuring a maximum skewness of 0.6. Figure 8 illustrates the implemented 3D mesh model.

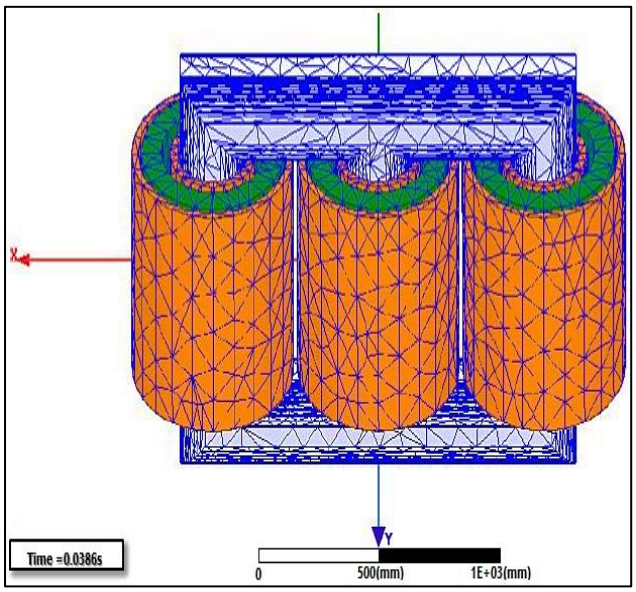

Fig 8: the 3D Mesh Model

Mesh refinement enhanced simulation accuracy which was crucial for accuracy of the results. Using the finite element field manager, electromagnetic force per unit volume and magnitude within phase windings were computed. Symmetric distribution of EMF and magnetic flux density along the axial direction was also observed. Opposing current directions between LV and HV windings resulted in inward force on LV winding and outward force on HV winding. Figure 9 shows the associated B-H characteristics curve of the selected core material (M6 steel) modeled using equation (38).

ISSN No:-2456-2165 https://doi.org/10.38124/ijisrt/IJISRT24MAY479

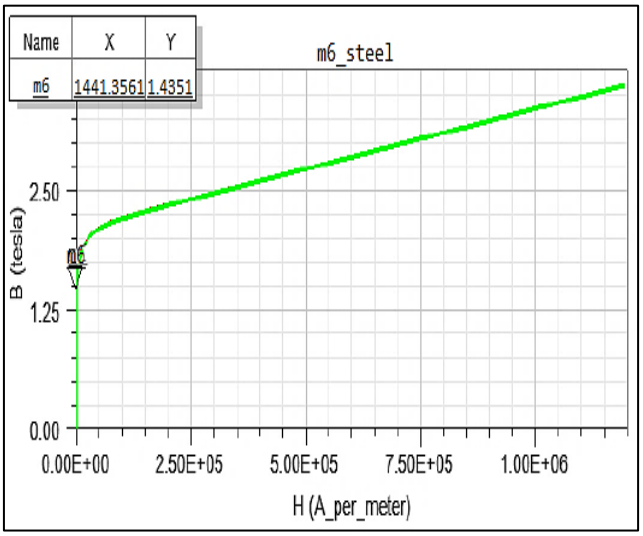

Fig 9: B-H Curve for the Selected Steel Core Material

G. The Experimental Set-up

The setup for ferroresonance investigation (shown in Figure 10) was anchored by a DE-LORENZO Transformer Experimental Set-Up (DL 10103TG), adhering to the IEC 61000-4-30 class A standard. With a power rating of 20 kVA and primary voltages spanning from 0.480 kV to 11 kV, the secondary voltages were set at 430V/230V and 208V/120V, operating at frequencies of 50/60 Hz. Voltage and current waveforms were recorded, with currents measured using embedded FOCUS™ coils and current clamps via the high-speed low voltage input, while voltages were directly measured via the high-speed high voltage input, all sampled at 20 kHz. The system integrates three phase line models as well as capacitive, inductive, and resistive loads, each comprising three components with configurable connections as shown by the schematic of Figure 11. The line models and variable loads allow precise adjustment of coupling capacitance, reactive power and voltage levels, crucial for conducting thorough investigations into ferroresonance phenomena. Data acquisition was enabled by an integrated (DL 1893) Interface Unit, offering a range of current measurements and accurate data acquisition capabilities.

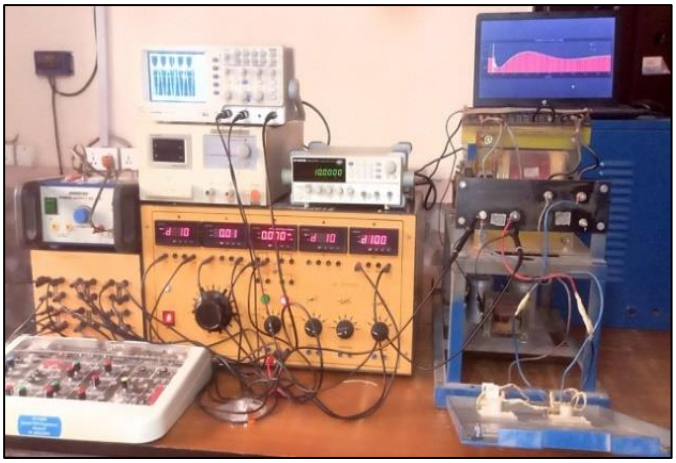
Fig 10: Experimental Set-up for the Study

The synchronized acquisition system boasted 4xHS-HV inputs, 4xHS-ACC inputs, and an ADC type of 16-bit SAR, supporting a sampling rate of up to 1 MS/s simultaneously. The HS-HV input provided a range of ±800 V with a bandwidth of 2 MHz, while the HS-ACC input offered a range of ±1 V with a bandwidth of 500 kHz.

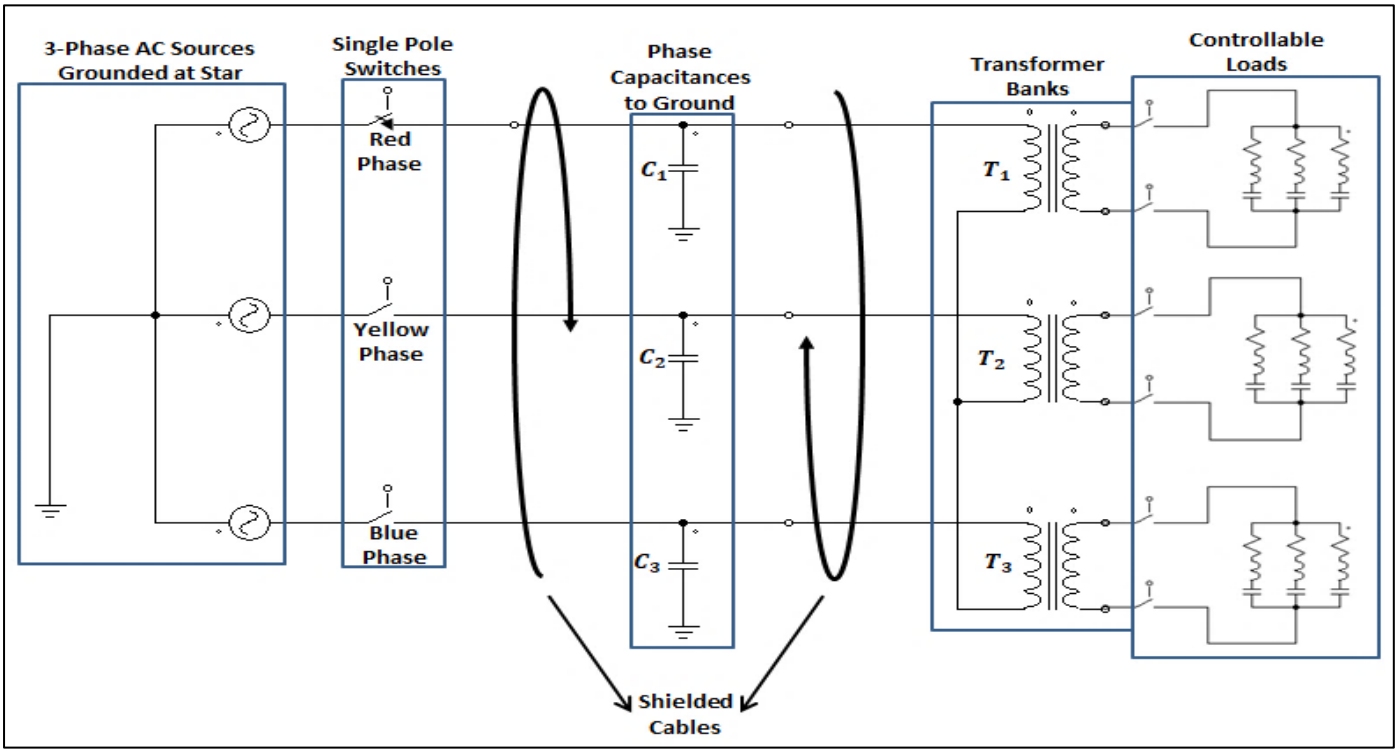

Fig 11: Schematic for the Experimental Set-up of Figure 8

ISSN No:-2456-2165 https://doi.org/10.38124/ijisrt/IJISRT24MAY479

IV. DISCUSSION OF RESULTS

A. FEM Simulation Results

Magnetic flux density distribution is simulated under no-load conditions. A 3D analysis using the time-stepping method shows flux density distribution in the transformer core under no-load conditions as seen in Figures 12 and 13. Time-Harmonic solver was used for the analysis, considering the complexity of core sheet overlap in the 3D model. The simulation results depicted in Figures 12 and 13 correspond to the time step when all three-phase ferroresonant currents reach their minimum values. Notably, there is no indication of core saturation in either of the transformers. However, a significant disparity exists in the flux density within the core: the baseline transformer (Figure 13) exhibits a flux density approximately 40% higher than that of the optimized transformer (Figure 12). The reason for the disparity in flux density between the baseline and optimized transformers is due to the core material properties. In the optimized transformer, the core material has been designed during FEM optimization with controlled additional iron core resistance (represented by the term $\frac{{X_m}^2 R_{fe}}{{R_{fe}}^2+{X_m}^2}$. This additional resistance effectively reduces the worst-case magnitudes of both voltage and current, as it shortens the ellipse in the ferroresonant circuit. As a result, the flux density in the optimized transformer core is lower compared to the baseline transformer, despite similar operating conditions. This controlled increase in core resistance helps mitigate the effects of ferroresonance and enhances the performance of the transformer under varying load conditions. Interestingly the core loss analysis from FEM simulations shows lower average core loss for the optimized transformer (Figure 14) than that of the baseline transformer (Figure 15).

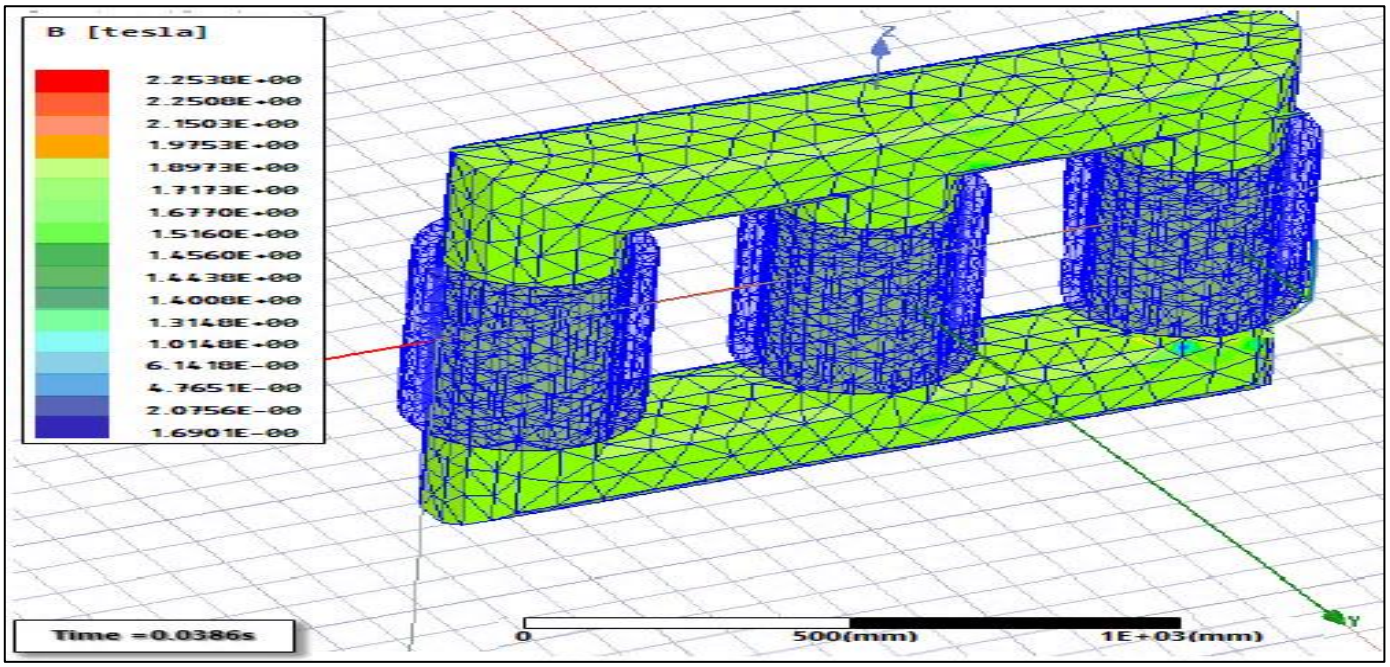

Fig 12: 3D Meshed Model of Optimized Transformer Showing Flux Density Distribution under No-Load Conditions

ISSN No:-2456-2165 https://doi.org/10.38124/ijisrt/IJISRT24MAY479

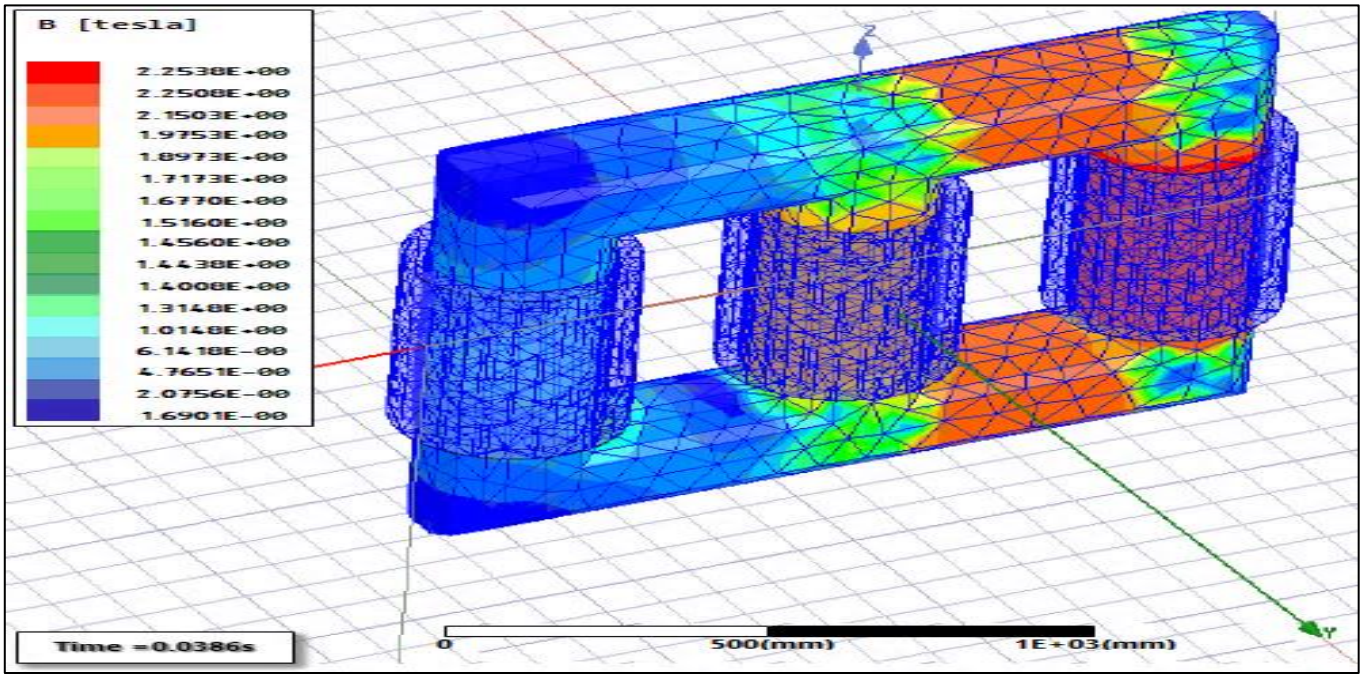

Fig 13: 3D Meshed Model of Baseline Transformer Showing Flux Density Distribution under No-Load Conditions

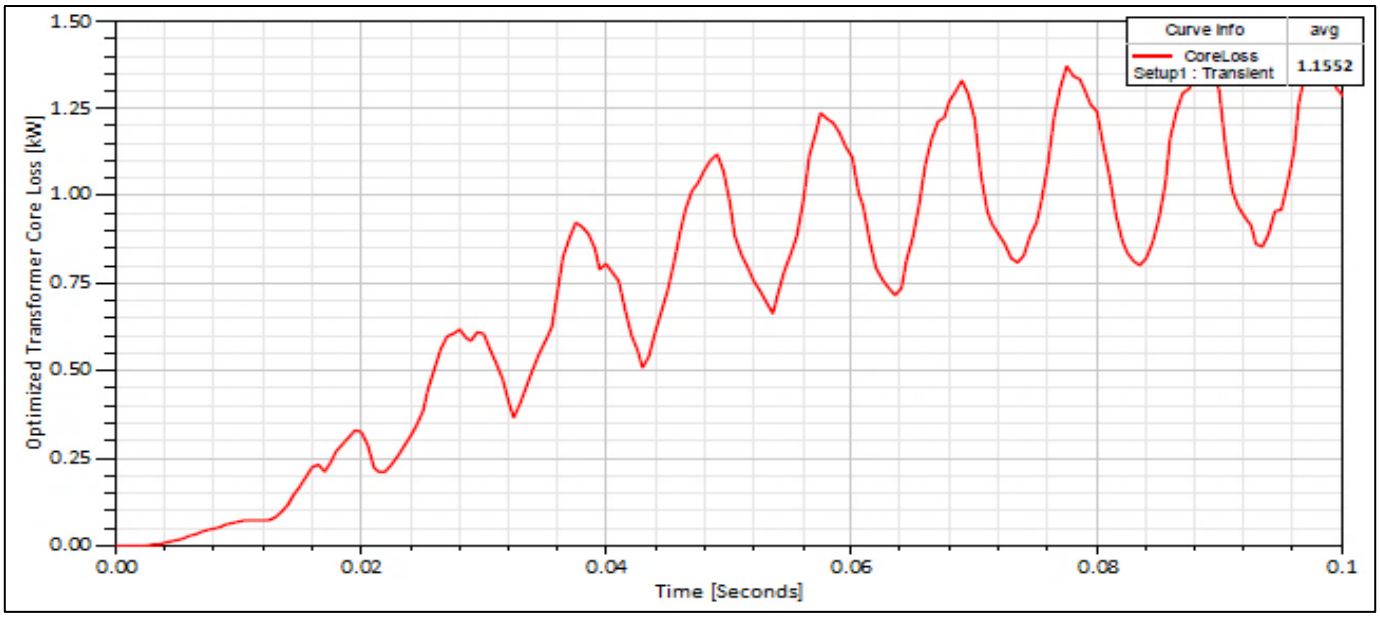

Fig 14: Optimized Transformer Core Loss Analysis

ISSN No:-2456-2165 https://doi.org/10.38124/ijisrt/IJISRT24MAY479

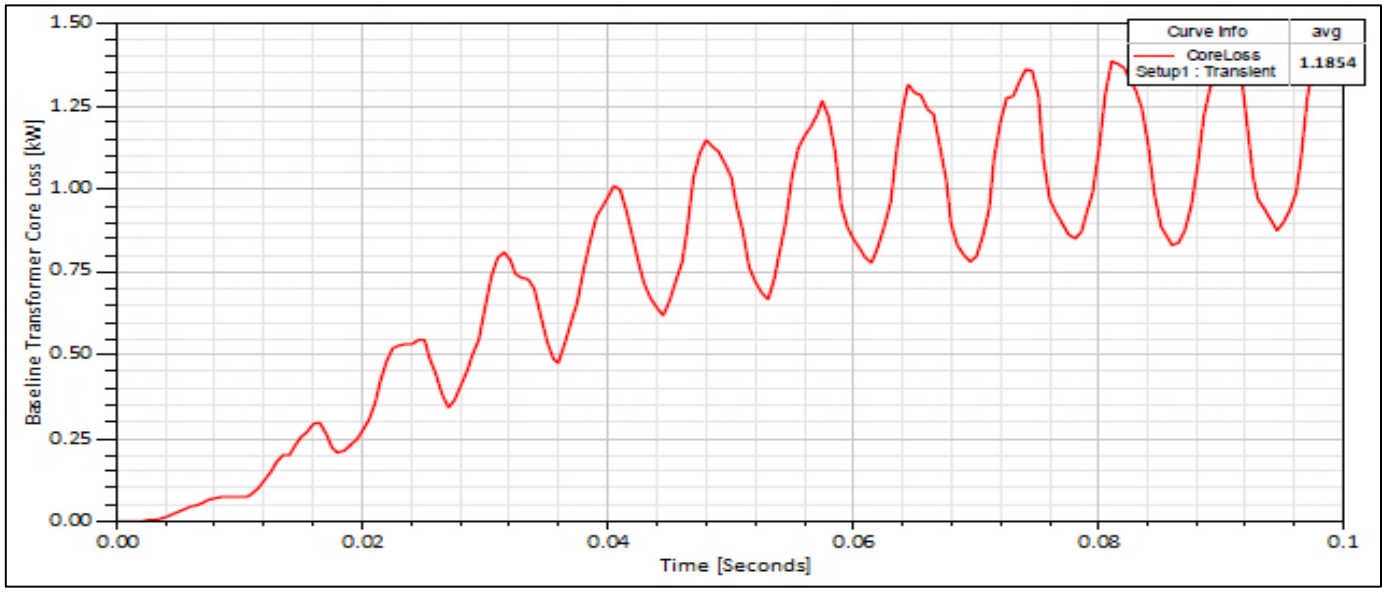

Fig 15: Baseline Transformer Core Loss Analysis

B. MATLAB/Simulink Simulation Results

The equivalent circuit of AC distribution system; as well as the generalized nonlinear inductance electromagnetic transformer (NI-EMT) Models were created using MATLAB/Simulink with SimPowerSystems to replicate diverse ferroresonance conditions and observe their impact on power system sinusoidal waveforms. The models were designed with simplicity and reproducibility in mind, utilizing default settings and minimizing the number of blocks to enhance their readability. Additionally, these models served as fundamental components for larger distribution system simulations. With a designated 2MVA, 33kV/11kV source feeder sub-station feeding the 11kV/0.415kV, 50Hz low voltage distribution system, the complete simulation model (shown in Figure 16) encompasses a range of disturbances including energized transformer, powered capacitor banks, ferroresonance transients block, and nonlinear loads. These simulations provide insights into various power quality issues and their effects on the system. The coupling capacitance was systematically varied to simulate diverse ferroresonance scenarios, directly influencing resonant interactions in the transformer and network. By varying capacitance values, realistic power system conditions were replicated. Additionally, configuring Capacitive, Inductive, and Resistive Loads in star, delta, and parallel arrangements enabled precise adjustment of load characteristics, facilitating thorough investigation of ferroresonance phenomena.

ISSN No:-2456-2165 https://doi.org/10.38124/ijisrt/IJISRT24MAY479

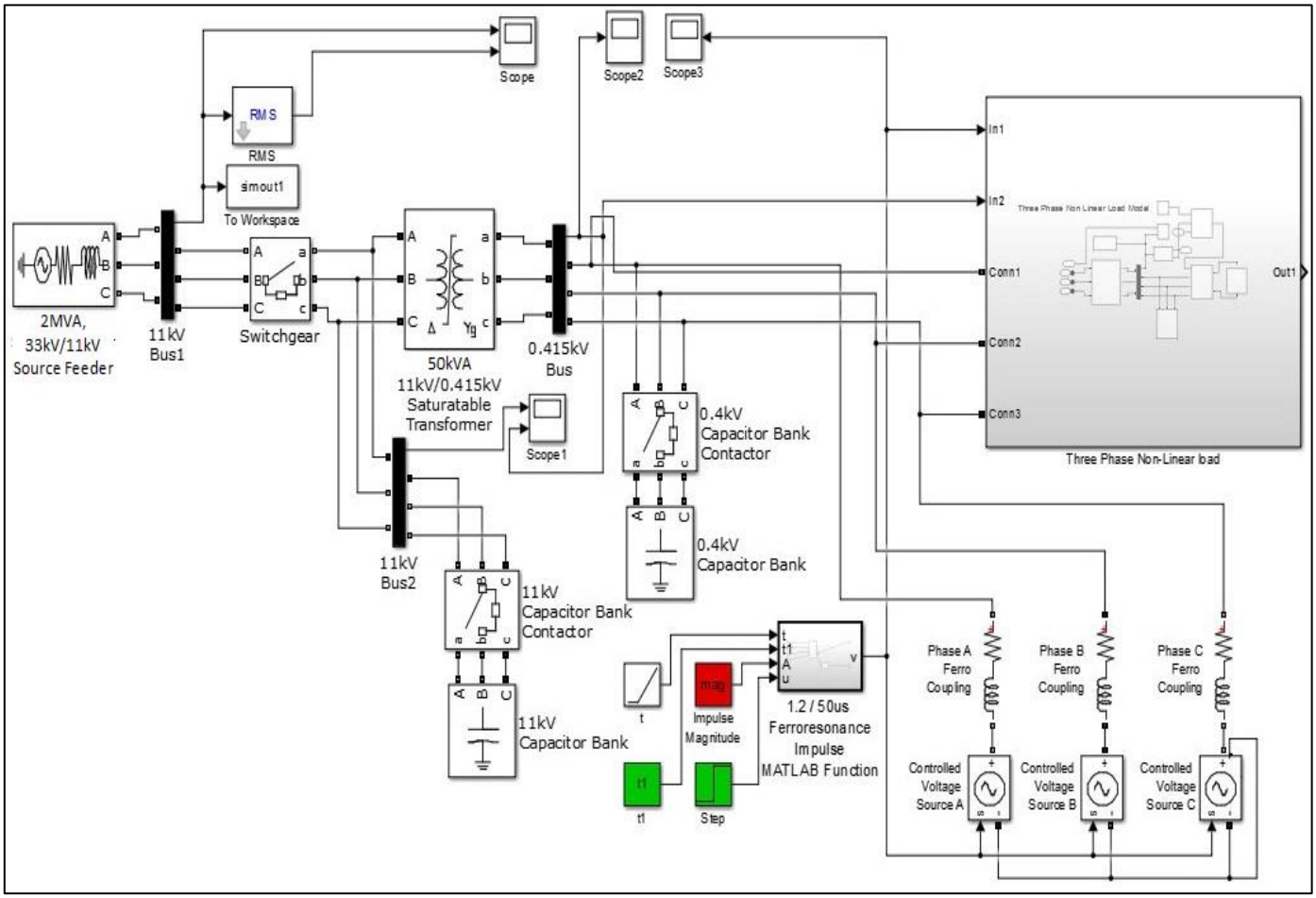

Fig 16: MATLAB/Simulink developed Models for Ferroresonance Investigation

- CASE I: The system was set to operate across different points with varying load requirements, primarily supplied from a 2MVA feeder transformer delta-connected on the HV side. The results were plotted over a duration of 0.06 seconds with a time step of 0.01 seconds. During initial no-load conditions (around 0.02 to 0.06 seconds into simulation), nonlinear loads resulting from residual flux in the transformer cores became predominant; and total harmonic distortions (THD) on the LV side of the baseline transformer increased to approximately 25 – 18%, yet remained below the threshold for inducing ferroresonance mode. Conversely, THD in the optimized transformer remained between 3.2 – 4.7% This is illustrated by Figures 17 and 18, where the optimized transformer exhibited minimal distortion in its voltage waveform (Figure 17), in contrast to the baseline transformer, which showed some distortion, notably of the 5th harmonics (Figure 18).

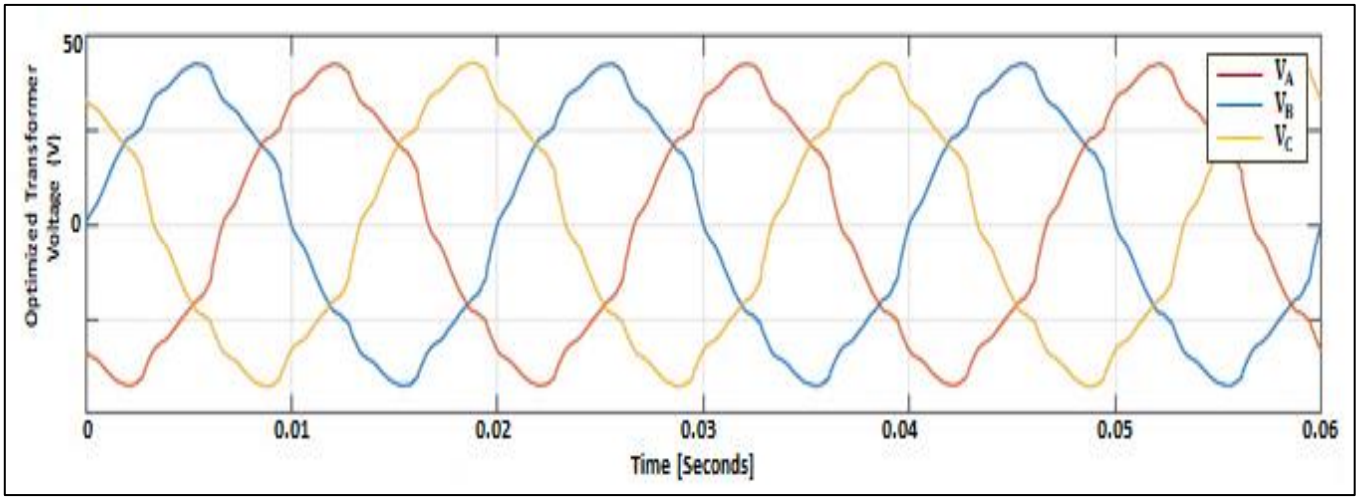

Fig 17: Optimized Transformer Voltage Waveform (Case I)

ISSN No:-2456-2165 https://doi.org/10.38124/ijisrt/IJISRT24MAY479

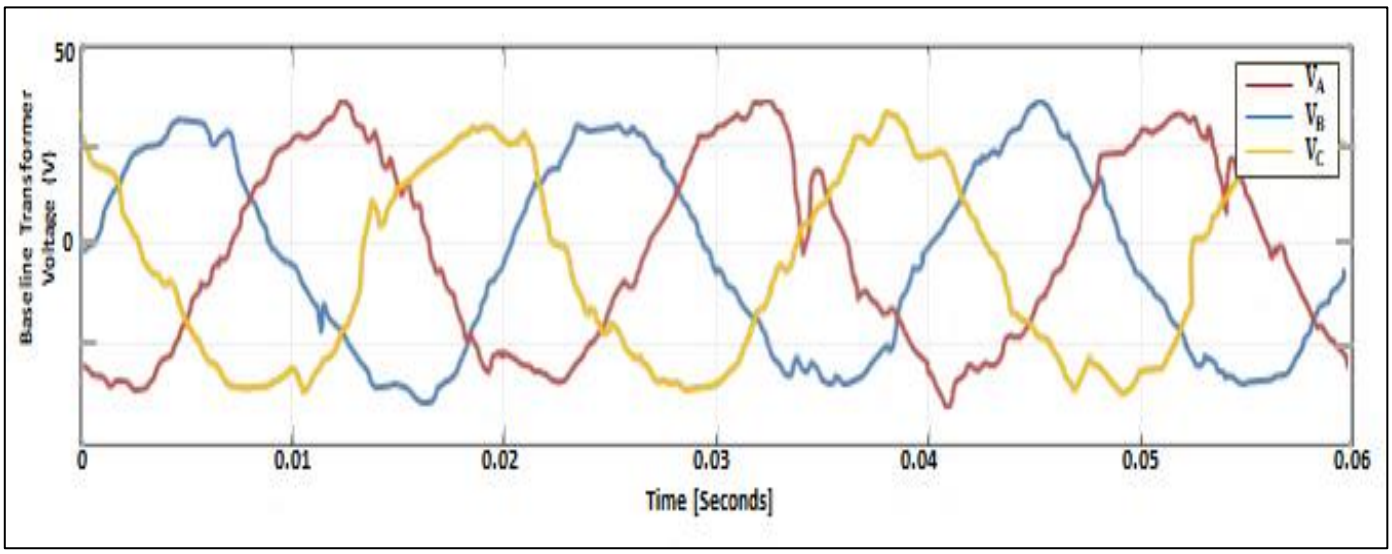

Fig 18: Baseline Transformer Voltage Waveform (Case I)

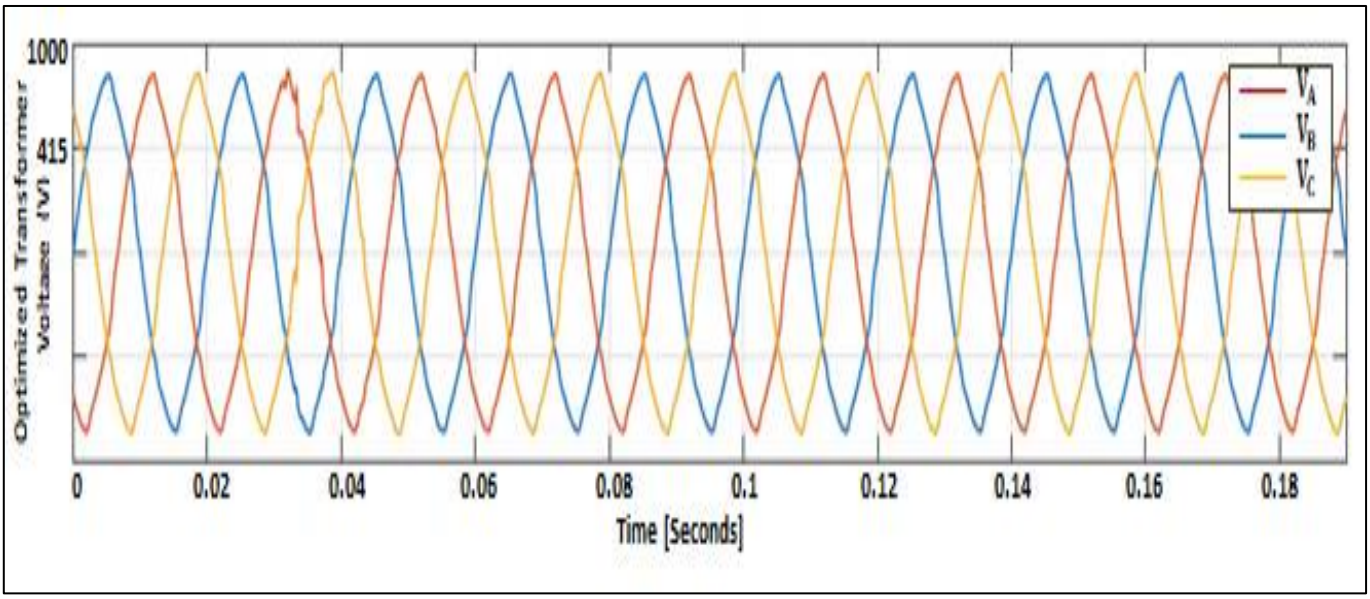

Fig 19: Optimized Transformer Voltage Waveform (Case II)

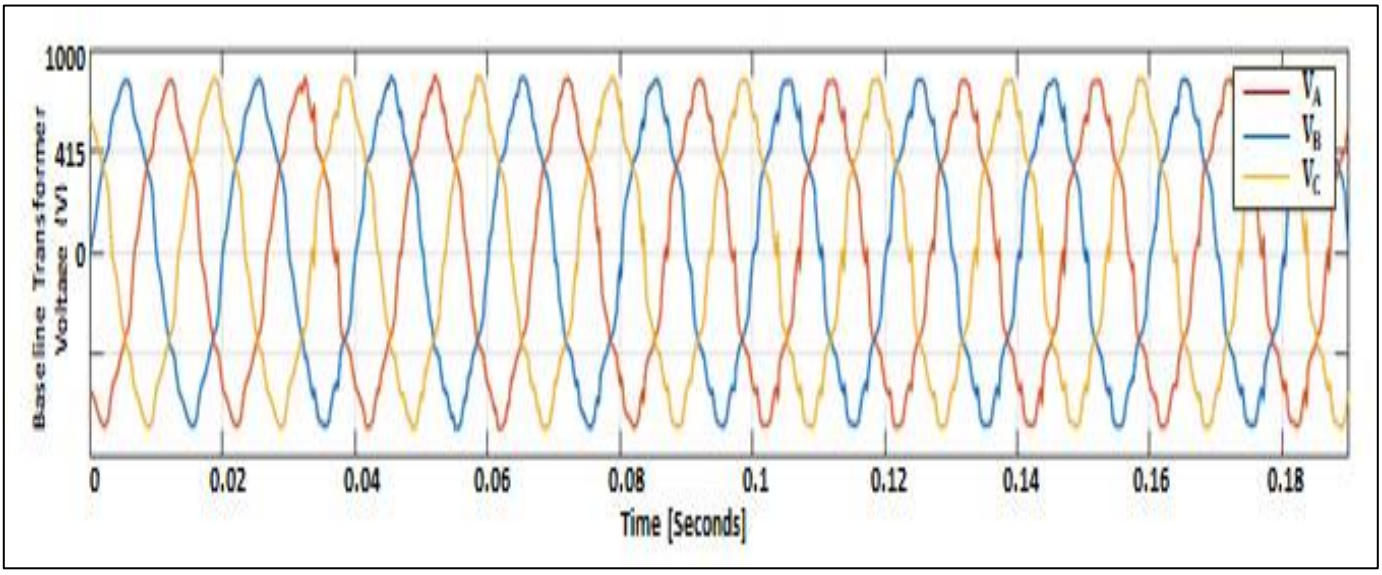

Fig 20: Baseline Transformer Voltage Waveform (Case II)

ISSN No:-2456-2165 https://doi.org/10.38124/ijisrt/IJISRT24MAY479

- CASE II: With Bus1, along with the 11kV capacitor bank contactor closed, Bus2, and the 0.415kV Bus initiated, additional nonlinear loads are introduced, along with the equivalent leakage inductances of the transformer ($a\psi + b\psi^n + \frac{\psi}{L_S}$). At some critical value of ferroresonance $\sum C\frac{d^2}{dt^2} = a\psi + b\psi^n + \frac{\psi}{L_0}$, a fundamental ferroresonance mode is triggered, as discussed earlier. System responses were observed over a 0.18-second duration with a time step of 0.02 seconds; and both transformers exhibit the onset of fundamental ferroresonance, as depicted in Figures 19 and 20. The voltage waveform of the optimized transformer (Figure 19) remains relatively unaffected, while the baseline transformer voltage waveform (Figure 20) shows distortion in discontinuous multiples of the fundamental harmonic.
- CASE III: Closing the 0.4kV capacitor bank contactor over a 0.18-second duration with a time step of 0.02 seconds; triggers a Ferroresonance transition into quasi/chaotic mode (as shown in Figures 21 through 26), depending on the selected load condition; as follows:
- Resistive Load of $10\Omega + Nominal\ Value = 10\Omega + 1688\Omega = 1698\Omega$ Rated at 5kW, Coupling Capacitance ($C_{coupling} = Nominal\ Value = 25.5\mu F$) (Figures 21 and 22)
- Resistive Load of $10\Omega + Nominal\ Value = 20\Omega + 1688\Omega = 17088\Omega$ Rated at 10kW, Coupling Capacitance ($C_{coupling} = Nominal\ Value + Supplementary\ Capacitive\ Banks = 25.5\mu F + 1\mu F = 26.5\mu F$) (Figures 23 and 24)
- Resistive Load of $20\Omega + Nominal\ Value = 20\Omega + 1688\Omega = 1708\Omega$ Rated at 15kW,Coupling Capacitance ($C_{coupling} = Nominal\ Value + Supplementary\ Capacitive\ Banks = 25.5\mu F + 8.5\mu F = 37\mu F$) (Figures 25 and 26)

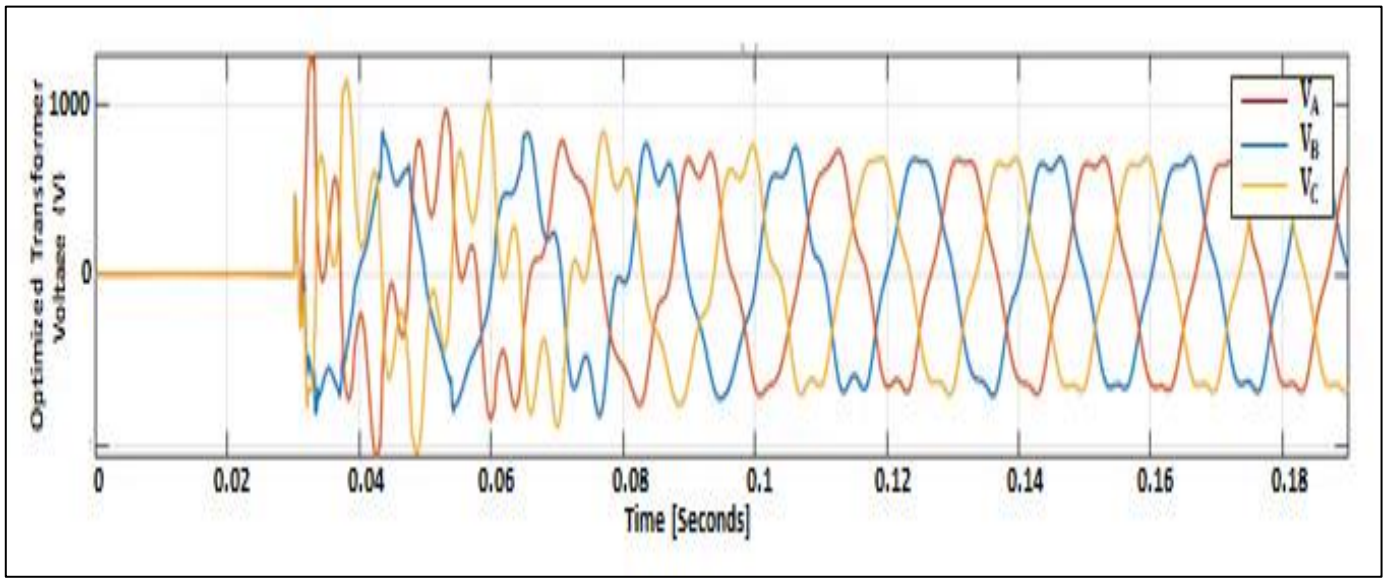

Fig 21: Optimized Transformer Voltage Waveform (Case III 'A')

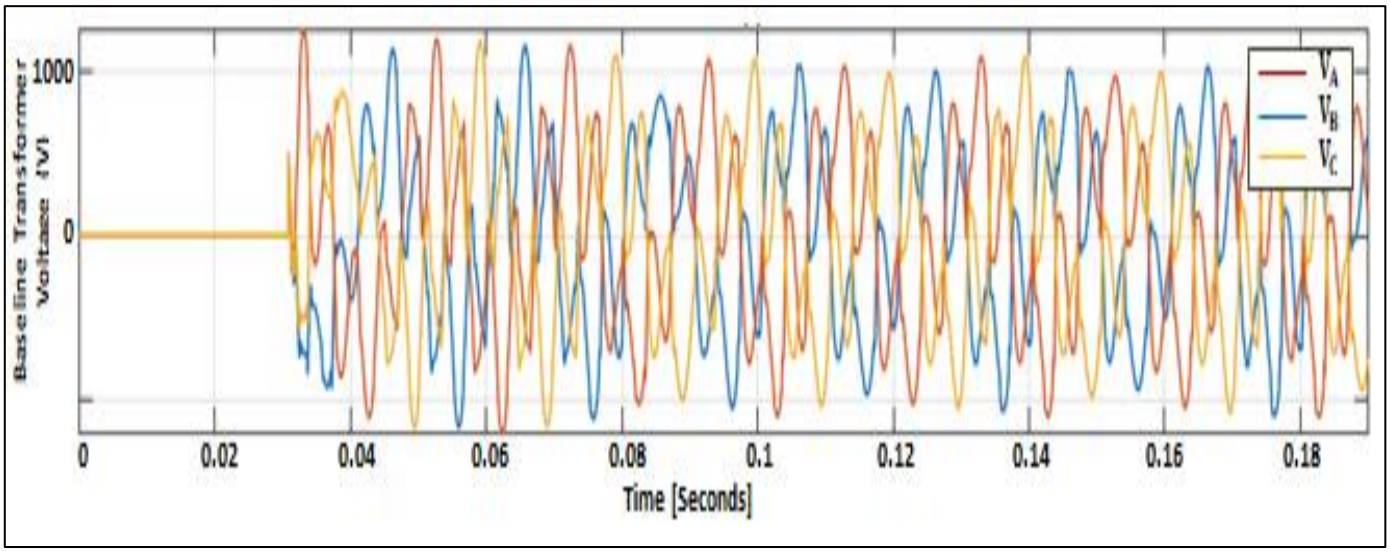

Fig 22: Baseline Transformer Voltage Waveform (Case III 'A')

ISSN No:-2456-2165 https://doi.org/10.38124/ijisrt/IJISRT24MAY479

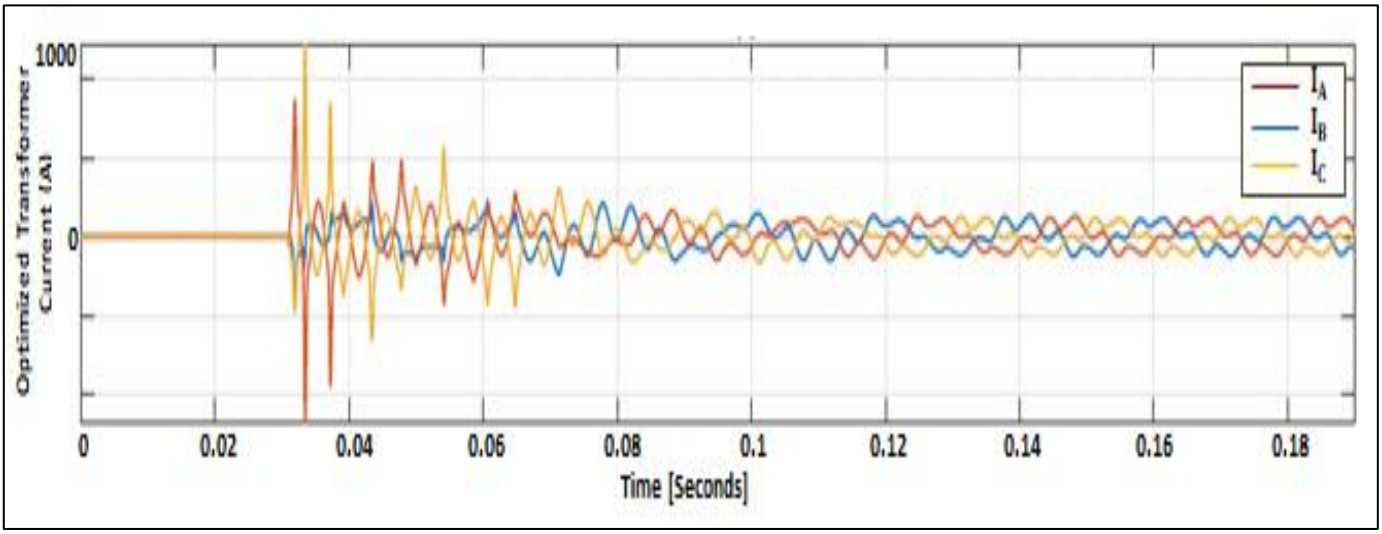

Fig 23: Optimized Transformer Voltage Waveform (Case III 'B'); Quasi Ferroresonance Mode

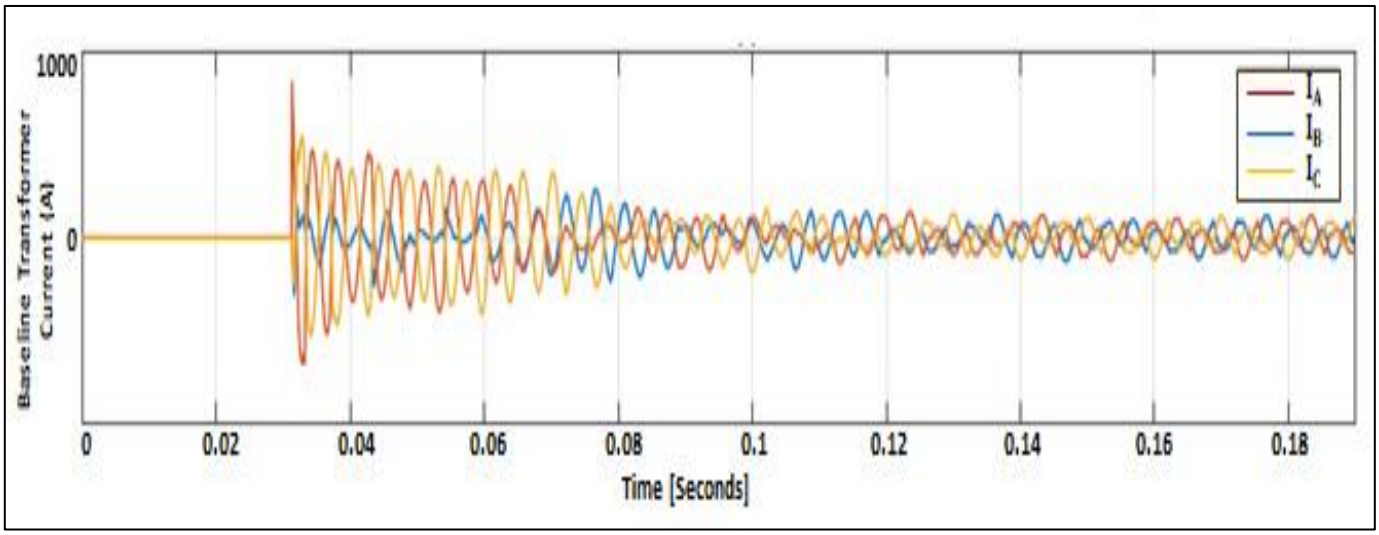

Fig 24: Baseline Transformer Current Waveform (Case III 'B'); Quasi Ferroresonance Mode

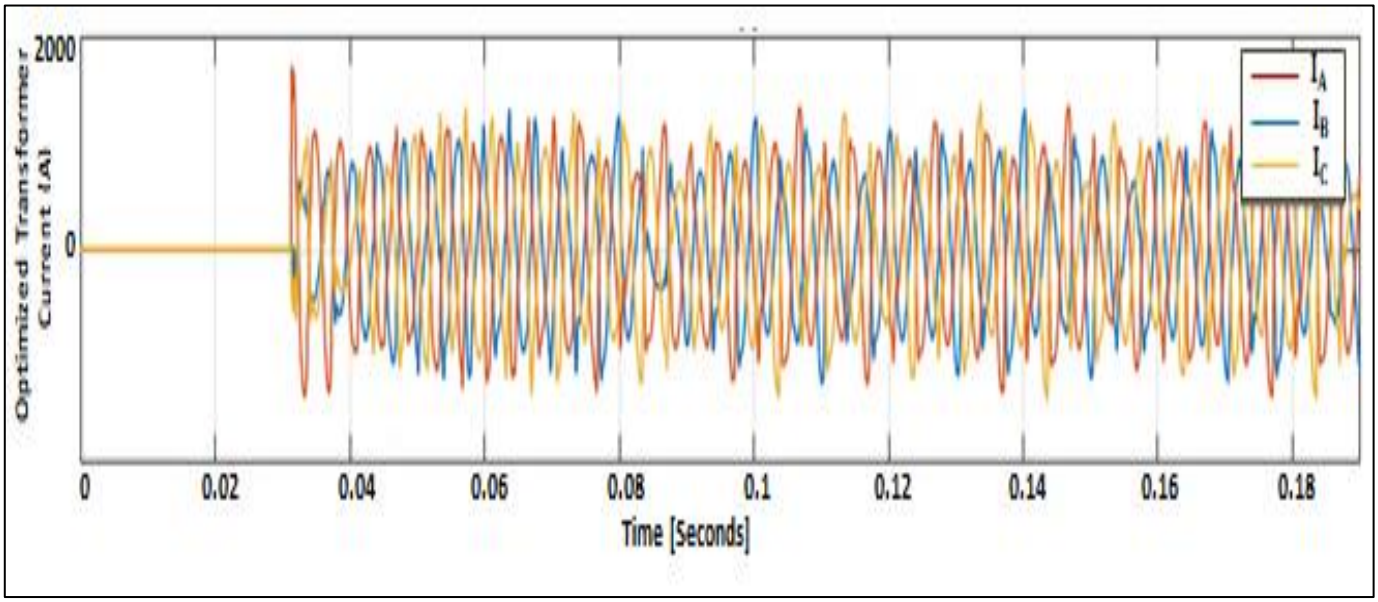

Fig 25: Optimized Transformer Current Waveform (Case III 'B'); Chaotic Ferroresonance Mode

ISSN No:-2456-2165 https://doi.org/10.38124/ijisrt/IJISRT24MAY479

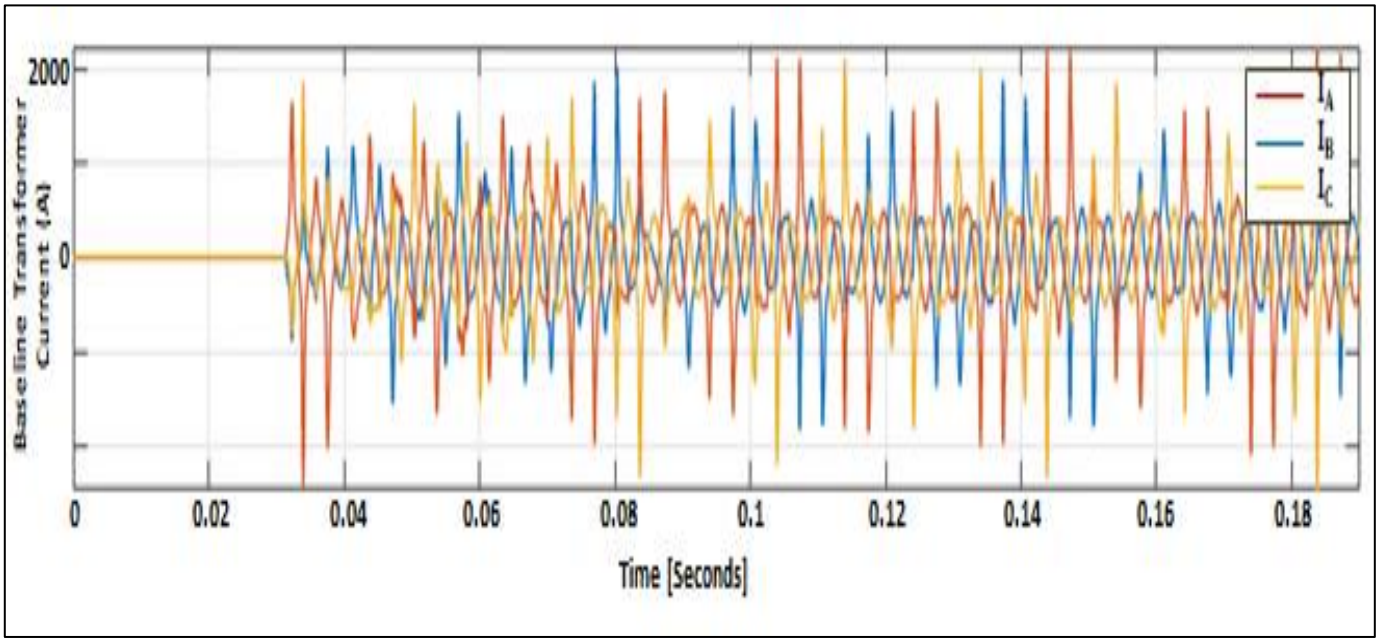

Fig 26: Baseline Transformer Current Waveform (Case III 'B'); Chaotic Ferroresonance Mode

V. CONCLUSIONS

This study aimed to comprehensively investigate transformer performance by integrating Finite Element Method (FEM) simulation with MATLAB/Simulink modeling and simulation. It focused on understanding efficiency, core losses, and ferroresonance phenomena, exploring transformer behaviors such as anisotropy and non-linearity. Grounded in the NIEMT Model and Maxwell's equations, the study modeled core losses, reluctivity, and relative permeability to capture magnetic flux dynamics. Additionally, MATLAB/Simulink models were utilized to simulate ferroresonance effects on distribution transformer behavior in low voltage power systems. The findings revealed notable differences in ferroresonance resilience between baseline and optimized transformers, with the latter demonstrating up to a 30% reduction in total harmonic distortion (THD). Furthermore, the optimized transformer exhibited significantly lower flux density and losses, with the baseline transformer showing 40% higher flux density and 2.55% higher losses. These results showcase the efficacy of design modifications in enhancing performance. The study's experimental validation emphasized practical implications, while ferroresonance analysis identified key stability challenges and potential mitigation strategies.

A. Practical and Theoretical Implications

The study holds implications for practical transformer design and theoretical understanding of electromagnetic phenomena. By integrating Finite Element Method (FEM) simulations with MATLAB/Simulink simulations, insights into transformer performance are provided. These findings can aid in developing more efficient and reliable transformers, benefiting power system stability and energy efficiency.

B. Limitations and Recommendations for Future Work

Acknowledging limitations, the study's models involved simplifications that may not fully represent real-world complexity. Expanding experimental validation across varied conditions and refining numerical models to include thermal effects and dynamic loading could enhance accuracy. Further research into advanced ferroresonance mitigation strategies, such as active damping techniques and novel transformer designs, could bolster system reliability.

ACKNOWLEDGMENTS

The authors gratefully acknowledge the support of the Tertiary Education Trust Fund (TETFund) for funding this research, enabling valuable contributions to the field of transformer performance analysis and enhancement.

REFERENCES

[1]. Roy, M., & Roy, C. K. (2009). A Study on Ferroresonance with Varying Initial Conditions using a Nonlinear Model of Transformer. In 2009 Third International Conference on Power Systems (pp. 213). Kharagpur, India: IEEE. DOI: 10.1109/ICPES.2009.5384247.

[2]. Hepziba, R. J., Balaji, G., Muralikrishna, R., & Rathinavel, S. (2024). A Case Study on Transformer Ferroresonance for Subsea Cable Connected 230 kV Substations using PSCAD. Electric Power Systems Research, 230, 110192. ISSN 0378-7796. https://doi.org/10.1016/j.epsr.2024.110192.

[3]. Abdul-Malek, Z., Mehranzamir, K., Salimi, B., Nabipour Afrouzi, H., & Vahabi Mashak, S. (2013). Investigation of Ferroresonance Mitigation Techniques in Voltage Transformer Using ATP-EMTP Simulation. Jurnal Teknologi, 64(4), 85–95. Retrieved from www.jurnalteknologi.utm.my.

ISSN No:-2456-2165 https://doi.org/10.38124/ijisrt/IJISRT24MAY479

[4]. Kutija, M. & Pravica, L. (2021). Effect of Harmonics on Ferroresonance in Low Voltage Power Factor Correction System - A Case Study. Applied Sciences, 11(10), 1-20. https://doi.org/10.3390/app11104322.

[5]. Koledowo, S. O., Ashigwuike, E. C. & Bawa, A. (2020). A Study of Ferroresonance in Underground Distribution Network for 15MVA, 33/11 kV Injection Substation. Nigerian Journal of Technology (NIJOTECH), 39(1), 219-227. http://dx.doi.org/10.4314/njt.v39i1.25.

[6]. Olguín-Becerril, M. A., Angeles-Camacho, C., & Fuerte-Esquivel, C. R. (2014). Ferroresonance in subharmonic 3rd mode in an inductive voltage transformer, a real case analysis. Electrical Power and Energy Systems, 61, 318–325. https://doi.org/10.1016/j.ijepes.2014.03.057.

[7]. Erbay, A. (2012). Parameter Study of Ferro-Resonance with Harmonic Balance Method. Supervised Degree Project in Parameter Study of Ferro-Resonance with Harmonic Balance Method. Stockholm, Sweden: Electric Power Systems. XR-EE-ES 2012:010.

[8]. Ang, S. P. (2010). Ferroresonance Simulation Studies of Transmission Systems. Doctoral dissertation, The University of Manchester, Faculty of Engineering and Physical Sciences, School of Electrical and Electronic Engineering. Retrieved from: https://core.ac.uk/download/pdf/40031831.pdf.

[9]. Ma, X., Jia, R., Liang, C., Du, H., Dong, X., & Ding, M. (2022). Study of Transformer Harmonic Loss Characteristic in Distribution Network Based on Field-Circuit Coupling Method. Sustainability, 14(20), 12975. https://doi.org/10.3390/su142012975.

[10]. Thinh, D. X., Halim, H. A., Liu, Z., & Phung, T. (2016). Voltage harmonic effect on losses in distribution transformers. In 2016 IEEE International Conference on Sustainable Green Technologies and Environmental Impact of ICT (ICSGTEIS) (pp. 1-4). IEEE. DOI: 10.1109/ICSGTEIS.2016.7885761.

[11]. Mokryani, G., Haghifam, M., Latafat, H., & Gharbali, A. A. (2010). Analysis of ferroresonance in a 20kV distribution network. In 2010 International Power and Energy Conference (PECon) (pp. 305-309). IEEE. DOI: 10.1109/PEITS.2009.5407008.

[12]. Rojas, R. E., Chaves, J. S., & Tavares, M. C. (2023). Ferroresonance mitigation for the unconventional rural electrification system. Electric Power Systems Research, 223, 109590. https://doi.org/10.1016/j.epsr.2023.109590.

[13]. Mousavi, S. A. (2015). Electromagnetic modelling of power transformers for study and mitigation of effects of GICs [Doctoral thesis, Royal Institute of Technology (KTH), School of Electrical Engineering, Division of Electromagnetic Engineering]. Teknikringen 33 SE–100 44 Stockholm, Sweden.

[14]. Ferreira, R. S. d. A., Picher, P., Meghnefi, F., Fofana, I., Ezzaidi, H., Volat, C., & Behjat, V. (2023). Reproducing Transformers' Frequency Response from Finite Element Method (FEM) Simulation and Parameters Optimization. Energies, 16(11), 4364. https://doi.org/10.3390/en16114364.

[15]. Mehboob, N. (2012). Hysteresis Properties of Soft Magnetic Materials (Doctoral dissertation). University of Vienna.

[16]. Sarac, V. (2017). FEM 2D and 3D design of transformer for core losses computation. In Scientific Proceedings XIV International Congress "Machines. Technologies. Materials." 2017 - Summer Session. Faculty of Electrical Engineering, University "Goce Delcev", R. Macedonia.

[17]. Chen, Y., & Pillay, P. (2002). An improved formula for lamination core loss calculations in machines operating with high frequency and high flux density excitation. In Conference Record of the 2002 IEEE Industry Applications Conference. 37th IAS Annual Meeting (Cat. No.02CH37344) (pp. 759-766 vol.2). Pittsburgh, PA, USA. DOI: 10.1109/IAS.2002.1042645.

[18]. Riemer, B., Lange, E., & Hamayer, K. (2013). Calculation of the flux density distribution of three phase five limb power transformers considering nonlinear material properties. COMPEL-The International Journal for Computation and Mathematics in Electrical and Electronic Engineering, 32(4), 1230-1243.

[19]. Digalovski, M., Petkovska, L., & Najdenkoski, K. (2013). Determination of three-phase transformer reactances with 3D finite element method. International Journal on Information Technology and Security, 4(2), 65-72.

[20]. Sudha, B., Praveen, L. S. & Vadde, A. (2022). Classification of Faults in Distribution Transformer Using Machine Learning. Materials Today: Proceedings, 58(1), 616-622. https://doi.org/10.1016/j.matpr.2022.04.514.

[21]. Agarwala, A., Tahsin, T., Ali, M. F., Sarker, S. K., Hussain, S., Das, A. S. K., Das, P., Hasan, M. M., Tasneem, Z., Islam, M. M., Islam, M. R., Badal, M. F. R. & Ahamed, M. H. (2024). Towards next generation power grid transformer for renewables: Technology review. Engineering Reports. Advance online publication. https://doi.org/10.1002/eng2.12848.

[22]. Worku, M. Y. (2022). Recent Advances in Energy Storage Systems for Renewable Source Grid Integration: A Comprehensive Review. Sustainability, 14(10), 1-18. https://doi.org/10.3390/su14105985.

[23]. Behdani, B., Allahbakhshi, M., & Tajdinian, M. (2021). On the Impact of Geomagnetically Induced Currents in Driving Series Capacitor Compensated Power Systems to Ferroresonance. International Journal of Electrical Power & Energy Systems, 125 (2), 106424. https://doi.org/10.1016/j.ijepes.2020.106424.

[24]. Huang, S.J. & Hsieh, C.H. (2013). Relation Analysis for Ferroresonance of Bus Potential Transformer and Circuit Breaker Grading Capacitance. International Journal of Electrical Power & Energy Systems, 51(10), 61-70. https://doi.org/10.1016/j.ijepes.2013.03.005.

[25]. Kraszewski, W., Syrek, P. & Mitoraj, M. (2022). Methods of Ferroresonance Mitigation in Voltage Transformers in a 30 kV Power Supply Network. Energies, 15(24), 1 - 17. https://doi.org/10.3390/en15249516.

ISSN No:-2456-2165 https://doi.org/10.38124/ijisrt/IJISRT24MAY479

[26]. Ding, N., Wang, Q., Chen, Y., Xie, P., Liu, Z., Zheng, H.T. & Sun, M. (2023). Applying Second Order Optimization to Deep Transformers with Parameter-Efficient Tuning. (Accessed online on 2/6/2023). Retrieved from https://openreview.net/forum?id=4Fi-5Jiyy5w.
[27]. Hamzaçebi, C. (2020). Taguchi Method as a Robust Design Tool. In Quality Control: Intelligent Manufacturing, Robust Design and Charts. doi: 10.5772/intechopen.94908.
[28]. Barua, A., Deb, P. K., Maheshwari, R. & Tekade, R. K. (2018). Statistical Techniques in Pharmaceutical Product Development. In R. K. Tekade (Ed.), Advances in Pharmaceutical Product Development and Research: Dosage Form Design Parameters (pp. 339-362). Academic Press.
[29]. Pramono, W.B., Wijaya, F.D., Hadi, S.P., Wahyudi, M.S. & Indarto, A. (2023). Designing Power Transformer Using Particle Swarm Optimization with Respect to Transformer Noise, Weight, and Losses. Designs, 7(31), 1-22. Doi:10.3390/designs7010031.
[30]. Hernandez, C., Lara, J., Arjona, M. A. & Melgoza-Vazquez, E. (2023). Multi-Objective Electromagnetic Design Optimization of a Power Transformer Using 3D Finite Element Analysis, Response Surface Methodology, and the Third Generation Non-Sorting Genetic Algorithm. Energies, 16(5), 1-21. https://doi.org/10.3390/en16052248.
[31]. Li, H., Han, L., He, B. & Yang, S. (2001). Application research based on improved genetic algorithm for optimum design of power transformers. In ICEMS'2001. Proceedings of the Fifth International Conference on Electrical Machines and Systems (IEEE Cat. No.01EX501) (pp. 242-245 vol.1). Shenyang, China. doi: 10.1109/ICEMS.2001.970657.
[32]. Zhang, K., Chen, W., Cao, X., Song, Z., Qiao, G. & Sun, L. (2018). Optimization Design Of High-Power High-Frequency Transformer Based On Multi-Objective Genetic Algorithm. In 2018 IEEE International Power Electronics and Application Conference and Exposition (PEAC) (pp. 1-5). Shenzhen, China. doi: 10.1109/PEAC.2018.8590371.
[33]. Kul, S., Tezcan, S. S., Duysak, H., & Celtek, S. A. (2022). FEM-based Modeling and Optimization of Dry-Type Transformers with Metaheuristic Algorithms. Technical Gazette, 29(5), 1678-1685. doi:10.17559/TV-20220114203522.
[34]. Azizian, D. & Gharehpetian, G. B. (2018). Split-winding transformer design using new hybrid optimization algorithm based on PSO and I-BB-BC. IET Science, Measurement & Technology, 12(7), 936-944. doi: 10.1049/iet-smt.2017.0118.